Genetic Manipulation to Stress Granule Components Modifies Neurodegeneration in *Drosophila* Models of Amyotrophic Lateral Sclerosis

By

Emily Sarkisian

B.S., University of Rhode Island, 2019

Thesis

Submitted in partial fulfillment of the requirements for the Degree of Master of Science in the Graduate Program of Biotechnology at Brown University

PROVIDENCE, RHODE ISLAND

MAY 2025

AUTHORIZATION TO LEND AND REPRODUCE THE THESIS

As the sole author of this thesis, I authorize Brown University to lend it to other institutions for the purpose of scholarly research.

Date 4/29/2025 Emily Sarkisian

Emily Sarkisian, Author

I further authorize Brown University to reproduce this thesis by photocopying or other means, in total or in part, at the request of other institutions or individuals for the purpose of scholarly research.

Date 4/29/2025 Emily Sarkisian

Emily Sarkisian, Author

This thesis by Emily Sarkisian is accepted in its present form by the Graduate Program in Biotechnology as satisfying the thesis requirements for the degree of Master of Science

Date 29 April 2025 Signature: 

Dr. Kristi A. Wharton, Advisor

Date 29 April 2025 Signature: 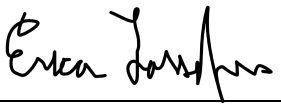

Dr. Erica Larschan, Reader

Date 29 April 2025 Signature: 

Dr. David Rand, Reader

Approved by the Graduate Council

Date _____ Signature: _____

Dr. Thomas Lewis, Dean of the Graduate School

Acknowledgments

I would like to thank my thesis advisor, Dr. Kristi Wharton, for her consistent guidance, encouragement, and space to further explore my interests in neurodegenerative disease. This transition from industrial research into academia was made easier through your mentorship and I am incredibly grateful for these past two years. Thank you to all of fellow lab members, past and current, for the laughs and companionship. Thank you to my thesis committee members, Dr. Erica Larschan and Dr. David Rand. Thank you also to the Director of the Biotechnology Master's Program, Dr. Jackie Schell. Thank you to our collaborators, especially to Dr. Anthony Vu and Dr. Gene Yeo at the University of California – San Diego as well as the Artavanis-Tsakonas Lab at Harvard University. Thank you to the National Institute of Neurological Disorders and Stroke for funding this research. Last but not least, thank you to my family and friends for their unconditional support.

Table of Contents

Table of Figures

Table of Tables

ABSTRACT

Abstract of Genetic Manipulation to Stress Granule Components Modifies Neurodegeneration in Drosophila *Models of Amyotrophic Lateral Sclerosis, by Emily Sarkisian, ScM, Brown University, May, 2025.*

Stress granules (SG) are membraneless, ribonucleoprotein structures that assemble as a protective response to stress in the cell. In the presence of chronic stress, SGs fail to dissolve, leading to persistent aggregation of proteins and stalled mRNA translation. SG dysfunction is a hallmark of many neurodegenerative diseases, including amyotrophic lateral sclerosis/frontotemporal dementia (ALS/FTD), yet it is unclear whether SG dysfunction is causative to these disorders or is in response to neurodegeneration.

Mutations to the genes *C9orf72* and *TARDBP* are seen in both sporadic and familial forms of ALS/FTD. We developed an adult-onset Drosophila model of *C9orf72-(G4C2)49* ALS, wherein adult flies exhibit a shortened lifespan and exacerbated decrease in climbing velocity with age. Using this and a motor neuron-driven *dTARDBP* patient allele (*TBPH[N493D]*), we tested if knocking down four SG-associated genes of interest using RNAi had any effect on neurodegeneration phenotypes in these two models. These genes (Heterogeneous nuclear ribonucleoprotein at 27C (*Hrb27C),* Tudor staphylococcal nuclease (*Tudor-SN*), maleless (*mle*), and ovarian tumor (*otu*)) were selected from a screen that identified ~150 novel human SG components (Markmiller et al., 2018). As shown previously, RNAi knockdown of each gene reduces a rough eye phenotype indicative of neurodegeneration when mutant human proteins are expressed in Drosophila photoreceptors (*GMR>hTDP-43[M337V] and hFUS[R521C]*). To better understand the extent to which these four SG genes alleviate neurotoxicity, we assessed ALS-associated defects in viability (eclosion), motor function (climbing), and survival (lifespan)

and how it may be modified by knockdown of each gene. The ability to suppress neurotoxicity associated with *C9orf72-(G4C2)49* ALS and *TBPH[N493D]* ALS models varied with each gene knockdown. We also assessed the pathological hallmark of TDP-43 ALS which includes toxic protein aggregation in the cytoplasm of the cell. We observe that knockdown of SG-associated genes can re-localize the protein to the nucleus. Our analysis highlights the dynamic role of SG-associated genes in ALS pathology.

Chapter 1 - INTRODUCTION

1.1 Amyotrophic Lateral Sclerosis (ALS)

Amyotrophic lateral sclerosis (ALS) is a progressive, neurodegenerative disease that is characterized by degeneration in upper and lower motor neurons (Brown & Al-Chalabi, 2017). The failure in upper motor neurons of the motor cortex result in spasticity and muscle stiffness whereas failure of lower motor neurons leads to eventual atrophy (Brown & Al-Chalabi, 2017; Hardiman et al., 2017). The disease has a central onset but progresses to other body regions (Masrori & Van Damme, 2020), where ultimate failure of the respiratory system limits a patient's survival to 2-5 years post-disease-onset (Brown & Al-Chalabi, 2017; Masrori & Van Damme, 2020). ALS has a lifetime risk of ~1:350 (Mead et al., 2023), with 5-10% of patients having a familial history of ALS (Brown & Al-Chalabi, 2017; Mead et al., 2023; Siddique & Ajroud-Driss, 2011). In addition to motor phenotypes, up to 50% of patients develop cognitive abnormalities – with up to 25% of these cases delivering a diagnosis of frontotemporal dementia (FTD) (Cividini et al., 2022). Males are also at a greater risk of developing the disease, especially in the European population (Manjaly et al., 2010).

It remains difficult to diagnose ALS in the clinic, with ALS encompassing a spectrum of symptoms. Many other neurodegenerative diseases present within this spectrum (Al-Chalabi et al., 2016). With no definitive diagnostic test for ALS, only clinical findings and exclusion of other neurodegenerative diseases, there is a blurry landscape for medical providers and patients (Al-Chalabi et al., 2016). For example, parkinsonism is an extramotor feature in ALS patients which could lead to some confusion in the clinic (Al-Chalabi et al., 2016; Lualdi et al., 2023). For these reasons, understanding the pathogenesis of ALS remains difficult for researchers.

1.2 Genes Associated with Amyotrophic Lateral Sclerosis

About 10% of all ALS cases are referred to as "familial" ALS, inherited either as autosomal dominant or as a recessive trait (Siddique & Ajroud-Driss, 2011; Wong et al., 1995). Over 100 gene mutations have been identified to cause an increased risk of developing ALS or modify the ALS phenotype (Ghasemi & Brown, 2018). The first ALS-associated mutation identified was in superoxide dismutase 1 (*SOD1*) in 1993 and has led to over 20 genes now being linked to ALS development (Ghasemi & Brown, 2018; Rosen et al., 1993; Yun & Ha, 2020). Across patient populations, the frequency of these mutations varies. However, the GGGGCC-hexanucleotide repeat expansion (G_4C_2 HRE) in the locus of chromosome 9 open reading frame 72 (*C9orf72*) is the most common mutation. As of 2020, it accounts for approximately 40% of familial cases and 7% of sporadic cases (Yun & Ha, 2020). The mutation in *SOD1*, which encodes a Cu/Zn-binding superoxide dismutase that catalyzes the reaction for superoxide to hydrogen peroxide and oxygen, is the second most common mutation observed (Rosen et al., 1993; Yun & Ha, 2020). Other commonly identified mutations occur in TAR DNA binding protein (*TARDBP*) and fused in sarcoma (*FUS)*. The proteins encoded by these genes are the DNA/RNA binding proteins TDP-43 and FUS, respectively (Ghasemi & Brown, 2018). Altogether, variations in *SOD1*, *C9orf72*, *FUS,* and *TARDBP* account for up to 60% of familial ALS cases and 10% of sporadic ALS cases (Yun & Ha, 2020).

As mentioned earlier, the definitive pathogenesis of ALS is still yet to be determined. Mutations in these ALS-associated genes have shown to be neurodegenerative. This extends not just to mammalian models, but across species. The mechanisms leading to neurodegeneration have a wide range of functions. TDP-43 transgenic mouse models have demonstrated that TDP-43 aggregation is not necessary to cause neurodegeneration seen in the models (Arnold et al.,

2013), highlighting that changes to just its role in splicing can occur without loss to nuclear TDP-43 or accumulation of aggregates. Work in *C. elegans* exhibited that different point mutations in *Sod1* lead to loss-of-function *and* gain-of-function toxic effects in glutamatergic and cholinergic neurons (Baskoylu et al., 2022). The protein C9ORF72 also functions as an autophagy regulator, as seen in patient-derived iPSCs (Webster et al., 2016). There are few definitive answers to what primarily drives the toxicity seen in ALS patients. How these previously described mutations lead to cellular toxicity is unclear. For more details on the *C9orf72* and *TARDBP* mutations please see section **1.5** and **1.6**.

1.3 ALS Pathogenesis

The mechanistic basis behind the onset and progression of ALS is still disputed as there are many pathways and molecular processes affected in available disease models and patients. Dysregulation of RNA metabolism, mitochondrial dysfunction, and protein homeostasis imbalance are just three of a number of pathological hallmarks seen in patient tissue (Zhou & Xu, 2023). The growth of the bioinformatics field and machine learning are providing an avenue to evaluate patient samples more broadly to observe patterns in tissue. A recent machine learning analysis utilized motor cortex samples from patients with sporadic ALS (sALS) (Marriott et al., 2023). Three biologically homogenous subgroups were identified: 1) synaptic and neuropeptide signaling, 2) oxidative stress and apoptosis, and 3) neuroinflammation. These three phenotypes have previously been identified using a multiomics approach in iPSC-derived *C9orf72*, *TARDBP*, *SOD1,* and *FUS* mutant motor neurons (Catanese et al., 2023). While this data is promising in order to narrow down specific pathways to analyze, other neurodegenerative

patient groupings were not tested meaning that these molecular phenotypes cannot be described as ALS-specific.

1.4 Modeling Neurodegeneration in *Drosophila Melanogaster*

The genome of the *Drosophila* is very well studied and provides a powerful genetic system to model disease. Many genes associated with human disease have an ortholog in the *Drosophila* genome, providing an easily-manipulated genetic model to work with. Its short lifespan is convenient to model age-related diseases, including ALS (Hales et al., 2015). Its nervous system is simpler compared to humans, but has well-defined centers for functions such as motor control (Jeibmann & Paulus, 2009; Kim et al., 2020; Lloyd & Taylor, 2010). In addition, the *Drosophila UAS/Gal4/Gal80* system allows for tissue and time-specific targeting of transgene expression. This can allow for transgenes being expressed specifically in motor neurons, for example (Walters et al., 2019). We are also able to drive targeted gene knockdown utilizing the RNA interference system (*RNAi*) (Dietzl et al., 2007). ALS studies utilizing *Drosophila* have exhibited reduced lifespans, locomotor defects, apoptosis, and impairment to neuronal populations which is in-line with mammalian ALS models (Fernius et al., 2017).

1.5 Hexanucleotide G4C2 HRE model of ALS in Drosophila

C9orf72 ALS is characterized by a HRE (Hexanucleotide Repeat Expansion) of GGGGCC (G_4C_2) in the first intron of the *C9orf72* locus (DeJesus-Hernandez et al., 2011; Renton et al., 2011). In healthy individuals, a normal range of 2-24 G_4C_2 repeats are present (van der Zee et al., 2013), however, toxicity associated with repeat expansion is generally observed when the number of repeats exceeds 30. While HRE is associated with neurotoxicity, there is

conflicting evidence as to any correlation between repeat length and age of disease onset or the severity of neurodegeneration and toxicity (Fournier et al., 2019; Gijselinck et al., 2016; Moron-Oset et al., 2023; van Blitterswijk et al., 2012). This HRE in the C9ORF72 intron results in two main toxic outcomes: a loss-of-function with haploinsufficiency, and a gain-of-function effect with expression of abnormally transcribed RNAs that carry the expanded repeat (DeJesus-Hernandez et al., 2011; Smeyers et al., 2021; van Blitterswijk et al., 2012). These RNAs accumulate to RNA foci or are translated into toxic dipeptide repeat proteins (DPRs) through repeat associated non-ATG (RAN) translation (Coyne et al., 2020; Lagier-Tourenne et al., 2013; Mori et al., 2013; Smeyers et al., 2021; Zu et al., 2013). Expressing 30 or more G_4C_2 repeats in the *Drosophila* eye using an ommatidial *GMR-Gal4* driver causes progressive degeneration of photoreceptors and results in a rough eye phenotype (Goodman et al., 2019; Xu et al., 2013). While the *GMR-Gal4* driver is used for "eye-specific" expression during *Drosophila* eye development, the GMR sequences drive gene expression in a number of other tissues during larval development (Li et al., 2012). And as ALS is primarily considered an adult-onset disease, we can utilize the *UAS-Gal4* system to activate the expression of G4C2 repeats in specific sets of cells within the adult to observe neurodegenerative effects of the G4C2 expansion (Mizielinska et al., 2014).

This thesis utilizes two models of *C9orf72* ALS – a 30X UAS-G_4C_2 (II) and a 49X UAS-G_4C_2 (II) repeat model (Goodman et al., 2019; Xu et al., 2013). The 30X model includes an *OK6-Gal4* (*Rapgap1)* motor neuron driver on the second chromosome (Sanyal, 2009). The 49X repeat model uses a pan-neuronal *nSyb-Gal4* (*neuronal Synaptobrevin)* driver, also on the second chromosome (Riabinina et al., 2015; Zappia & Frolov, 2016). Expression of 30X or 49X G4C2 repeats with either of these drivers causes a toxic, mutant phenotype.

1.6 *dTDP-43[N493D] Drosophila* ALS model

TAR DNA/RNA binding Protein 43 kDa (TDP-43) is encoded by the human gene *TARDBP*. Its role is essential for RNA splicing and cellular metabolism. TDP-43 protein aggregation is a hallmark feature of familial and sporadic ALS, with its presence observed in ~97% of all ALS patients regardless of disease onset mechanism. This does not include mutations in *SOD1* or *FUS* (Mackenzie et al., 2007; Mackenzie et al., 2010). Some TDP-43 missense mutations enhance the mislocalization of TDP-43 from the nucleus to the cytoplasm whereas others promote larger and/or abnormal stress granules (Jo et al., 2020). The toxic effects seen with presence of TDP-43 inclusions could result from the aggregation preventing traditional cellular activity. It has also been shown that the accumulation of cytoplasmic aggregates of TDP-43 lend to depletion of nuclear TDP-43 (Winton et al., 2008; Zhang et al., 2009). It has also been shown in a *Drosophila* model of TDP-43 that increases to cytosolic calcium levels lend to a decrease of cytoplasmic localization of TDP-43 (Park et al., 2020). Extensive work has been completed to map out clinical ALS progression and the neurotoxic role that mutated TDP-43 has (Braak et al., 2013; Brettschneider et al., 2013).

The ALS-mutations observed in ALS and FTD patients are present in the glycine-rich C-terminal domain of TARDBP, which demonstrates a pathogenic role in both of these diseases (Arnold et al., 2013). However, there are further mutations that have been identified in the related genes, fused in sarcoma (FUS) and translocated in liposarcoma (TLS) which point to defects in RNA processing itself that progresses ALS pathogenesis (Arnold et al., 2013; Kwiatkowski et al., 2009). There are also additional links to TDP-43 pathology and the accumulation of toxic DPRs that are also observed in patients with mutations in *C9orf72*. For

example, the translation of poly(GR) (glycine-arginine repeat protein) from the HRE in *C9orf72* has been shown to be capable of promoting TDP-43 aggregation. Toxic poly(GR) proteins are also capable of mediating sequestration of full-length TDP-43 in an RNA-independent manner to promote TDP-43 inclusions in the cytoplasm (Cook et al., 2020).

This thesis utilizes a *Drosophila* TDP-43 model of disease – *dTDP-43[N493D]*. For this model, there is an insertion of mutated *TBPH* which is the *Drosophila* homolog of *TARDBP*. This insertion is on the third chromosome. Along with a *UAS* regulatory sequence and a N493D point mutation in *TBPH*, it is an equivalent mutation to the human *TARDBP[N378D]* mutation (Kankel et al., 2020). The *TARDBP[N378D]* has been shown to be one such mutation in *TARDBP* that results in abnormal proteostasis and toxic accumulation of predominantly nuclear TDP-43 protein in the cytoplasm (Buratti, 2015; Watanabe et al., 2013). A motor neuron driven *TBPH[N493D]* mutation in *Drosophila* results in morphological defects in the neuromuscular junction (NMJ) as well as larval lethality (Kankel et al., 2020). In this model, the mutated TDP-43 protein is overexpressed as seen in an ALS patient with an *OK371-Gal4 (Drosophila vehicular glutamate transporter)* motor neuron driver (Mahr & Aberle, 2006).

1.7 Stress Granule Dynamics in ALS

Aberrant stress granule (SG) dynamics are a hallmark of ALS pathology. SGs are cytoplasmic, membrane-less organelles that are formed by liquid-liquid phase separation (LLPS) (Wheeler et al., 2016; Wolozin & Ivanov, 2019). These aggregates are primarily comprised or ribonucleoproteins (RNPs) and are formed in response to cellular stress, and will disassemble when the cellular stress is resolved. While samples from ALS patient indicate the brain and spinal cord to have higher numbers of SGs, it is undetermined whether these granules are

contributing to disease pathogenesis or are a consequential effect of the stress incurred by neurodegeneration (Dudman & Qi, 2020; Markmiller et al., 2018; Wolozin & Ivanov, 2019). It is also unclear whether this elevated presence of stress granules is due to greater production of SGs, a slow-down in disassembly of SGs, or a mix of both. There are variations in the composition of SGs, especially due to the type of cellular stress. It is also undetermined whether the components of the stress granules are relative to the degree of toxicity caused by the disassembly (Wolozin & Ivanov, 2019).

Our collaborators at the University of California, San Diego in Dr. Gene Yeo's lab identified 150-novel protein components in isolated stress granules (Markmiller et al., 2018). They determined that knockdown of *Drosophila* orthologs of several of the genes encoding these proteins suppressed an eye phenotype caused by overexpressing the mutant form of human TDP-43 (*hTDP-43[M337V]*) under the control of the GMR-Gal4 driver. They found that genetic manipulations of these SG genes could achieve a similar suppression of a second ALS model, *GMR-Gal4* driven human FUS with a patient mutation (*hFUS[R521C]*). Among the selected genes were OTUD4, DAZAP1, SND, and DHX9, *Drosophila melanogaster* orthologs *ovarian tumor* (*otu*)*, Heterogeneous Nuclear Ribonucleoprotein at 27C* (*Hrb27C*), *Tudor Staphylococcal Nuclease* (*Tudor-SN*), and *maleless* (*mle*), respectively. Interestingly, these genes encode proteins that have a wide range of functions, affecting a variety of cellular pathways.

An important component of stress granules are the nucleators which are components that are responsible for recruiting or stabilizing the core of these granules. Previous analysis has shown that these nucleators are required for the transition of pre-initiation complexes to SGs by directly binding to particular mRNAs or interacting with translation machinery (Markmiller et al., 2018; Wolozin & Ivanov, 2019). Others are capable of playing associating roles through their

known interactions with their mRNA targets. While screens have identified hundreds of proteins known to associate to stress granules, there are only limited contributors characterized as forming the SG 'core' (Markmiller et al., 2018; Wheeler et al., 2017; Wheeler et al., 2016; Wolozin & Ivanov, 2019). It is also important to understand the dynamic nature of SGs. The response time of stress granules is rapid, but is also dependent on the source of the stress as well as the components of the responding SG body. For example, the residence time of TIA1 has been reported to be seconds whereas FMRPs timing has been recorded as minutes (Antar et al., 2004; Kedersha et al., 2000; Wolozin & Ivanov, 2019). The four genes of interest in this thesis have not been identified as core nucleators in SGs, but instead may reflect associations with a subset of SGs, or a component of SGs only under certain stress conditions.

1.8 Master's Thesis

My thesis research highlights the role of stress granule-associated genes in two disease models, C9ORF72 and TDP-43. The SG genes we examined had previously demonstrated successful rescue of a neurodegeneration model in *Drosophila* which takes advantage of the degeneration of photoreceptor neurons in the eye, a tissue whose structure and function are not essential for organismal survival in the lab. Screening for suppression of a rough eye phenotype associated with the expression of human disease genes harboring patient alleles is a straightforward approach, however, it is possible that photoreceptors do not share the same physiology as other types of neurons more specifically affected in different neurodegenerative disease. In an attempt to better understand the cellular process that are affected not only by diseases such as ALS or FTD, but also by associated genetic knockdowns, we made use of other

in vivo models that more accurately recapitulate the disease state, to assess impact on nervous system function.

We used multiple genetic drivers to assess effects in specific cellular populations. In our *C9ORF72* model, I assessed the climbing velocity and median lifespan with 49 repeats of GGGGCC expressed pan-neuronally with a *nSyb-Gal4* driver. I also assessed adult viability in a model with 30 repeats of GGGGCC with a motor neuron *OK6-Gal4* driver. In a TDP-43 model with an overexpression of mutated *TBPH* in motor neurons, I measured adult viability and TBPH localization in motor neurons with an *OK371-Gal4* driver. I also assessed whether manipulations to calcium channels have the potential to rescue any defects observed in the *OK371>TBPH[N493D]* model.

1.9 References

Al-Chalabi, A., Hardiman, O., Kiernan, M. C., Chio, A., Rix-Brooks, B., & van den Berg, L. H. (2016). Amyotrophic lateral sclerosis: moving towards a new classification system. *Lancet Neurol*, *15*(11), 1182-1194. https://doi.org/10.1016/S1474-4422(16)30199-5

Antar, L. N., Afroz, R., Dictenberg, J. B., Carroll, R. C., & Bassell, G. J. (2004). Metabotropic glutamate receptor activation regulates fragile x mental retardation protein and FMR1 mRNA localization differentially in dendrites and at synapses. *J Neurosci*, *24*(11), 2648-2655. https://doi.org/10.1523/JNEUROSCI.0099-04.2004

Arnold, E. S., Ling, S. C., Huelga, S. C., Lagier-Tourenne, C., Polymenidou, M., Ditsworth, D., Kordasiewicz, H. B., McAlonis-Downes, M., Platoshyn, O., Parone, P. A., Da Cruz, S., Clutario, K. M., Swing, D., Tessarollo, L., Marsala, M., Shaw, C. E., Yeo, G. W., & Cleveland, D. W. (2013). ALS-Linked TDP-43 mutations produce aberrant RNA splicing and adult-onset motor neuron disease without aggregation or loss of nuclear TDP-43. *PNAS*, E736-E745. https://doi.org/10.1073/pnas.1222809110

Baskoylu, S. N., Chapkis, N., Unsal, B., Lins, J., Schuch, K., Simon, J., & Hart, A. C. (2022). Disrupted autophagy and neuronal dysfunction in C. elegans knockin models of FUS amyotrophic lateral sclerosis. *Cell Rep*, *38*(4), 110195. https://doi.org/10.1016/j.celrep.2021.110195

Braak, H., Brettschneider, J., Ludolph, A. C., Lee, V. M., Trojanowski, J. Q., & Del Tredici, K. (2013). Amyotrophic lateral sclerosis--a model of corticofugal axonal spread. *Nat Rev Neurol*, *9*(12), 708-714. https://doi.org/10.1038/nrneurol.2013.221

Brettschneider, J., Del Tredici, K., Toledo, J. B., Robinson, J. L., Irwin, D. J., Grossman, M., Suh, E., Van Deerlin, V. M., Wood, E. M., Baek, Y., Kwong, L., Lee, E. B., Elman, L., McCluskey, L., Fang, L., Feldengut, S., Ludolph, A. C., Lee, V. M., Braak, H., &

Trojanowski, J. Q. (2013). Stages of pTDP-43 pathology in amyotrophic lateral sclerosis. *Ann Neurol*, *74*(1), 20-38. https://doi.org/10.1002/ana.23937

Brown, R. H., & Al-Chalabi, A. (2017). Amyotrophic Lateral Sclerosis. *N Engl J Med*, *377*(2), 162-172. https://doi.org/10.1056/NEJMra1603471

Buratti, E. (2015). Functional Significance of TDP-43 Mutations in Disease. *Adv Genet*, *91*, 1-53. https://doi.org/10.1016/bs.adgen.2015.07.001

Catanese, A., Rajkumar, S., Sommer, D., Masrori, P., Hersmus, N., Van Damme, P., Witzel, S., Ludolph, A., Ho, R., Boeckers, T. M., & Mulaw, M. (2023). Multiomics and machine-learning identify novel transcriptional and mutational signatures in amyotrophic lateral sclerosis. *Brain*, *146*(9), 3770-3782. https://doi.org/10.1093/brain/awad075

Cividini, C., Basaia, S., Spinelli, E. G., Canu, E., Castelnovo, V., Riva, N., Cecchetti, G., Caso, F., Magnani, G., Falini, A., Filippi, M., & Agosta, F. (2022). Amyotrophic Lateral Sclerosis-Frontotemporal Dementia: Shared and Divergent Neural Correlates Across the Clinical Spectrum. *Neurology*, *98*(4), e402-e415. https://doi.org/10.1212/WNL.0000000000013123

Cook, C. N., Wu, Y., Odeh, H. M., Gendron, T. F., Jansen-West, K., Del Rosso, G., Yue, M., Jiang, P., Gomes, E., Tong, J., Daughrity, L. M., Avendano, N. M., Castanedes-Casey, M., Shao, W., Oskarsson, B., Tomassy, G. S., McCampbell, A., Rigo, F., Dickson, D. W.,…Petrucelli, L. (2020). C9orf72 poly(GR) aggregation induces TDP-43 proteinopathy. *Sci Transl Med*, *12*(559). https://doi.org/10.1126/scitranslmed.abb3774

Coyne, A. N., Zaepfel, B. L., Hayes, L., Fitchman, B., Salzberg, Y., Luo, E. C., Bowen, K., Trost, H., Aigner, S., Rigo, F., Yeo, G. W., Harel, A., Svendsen, C. N., Sareen, D., & Rothstein, J. D. (2020). G(4)C(2) Repeat RNA Initiates a POM121-Mediated Reduction in Specific Nucleoporins in C9orf72 ALS/FTD. *Neuron*, *107*(6), 1124-1140 e1111. https://doi.org/10.1016/j.neuron.2020.06.027

DeJesus-Hernandez, M., Mackenzie, I. R., Boeve, B. F., Boxer, A. L., Baker, M., Rutherford, N. J., Nicholson, A. M., Finch, N. A., Flynn, H., Adamson, J., Kouri, N., Wojtas, A., Sengdy, P., Hsiung, G. Y., Karydas, A., Seeley, W. W., Josephs, K. A., Coppola, G., Geschwind, D. H.,…Rademakers, R. (2011). Expanded GGGGCC hexanucleotide repeat in noncoding region of C9ORF72 causes chromosome 9p-linked FTD and ALS. *Neuron*, *72*(2), 245-256. https://doi.org/10.1016/j.neuron.2011.09.011

Dietzl, G., Chen, D., Schnorrer, F., Su, K. C., Barinova, Y., Fellner, M., Gasser, B., Kinsey, K., Oppel, S., Scheiblauer, S., Couto, A., Marra, V., Keleman, K., & Dickson, B. J. (2007). A genome-wide transgenic RNAi library for conditional gene inactivation in Drosophila. *Nature*, *448*(7150), 151-156. https://doi.org/10.1038/nature05954

Dudman, J., & Qi, X. (2020). Stress Granule Dysregulation in Amyotrophic Lateral Sclerosis. *Front Cell Neurosci*, *14*, 598517. https://doi.org/10.3389/fncel.2020.598517

Fernius, J., Starkenberg, A., & Thor, S. (2017). Bar-coding neurodegeneration: identifying subcellular effects of human neurodegenerative disease proteins using Drosophila leg neurons. *Dis Model Mech*, *10*(8), 1027-1038. https://doi.org/10.1242/dmm.029637

Fournier, C., Barbier, M., Camuzat, A., Anquetil, V., Lattante, S., Clot, F., Cazeneuve, C., Rinaldi, D., Couratier, P., Deramecourt, V., Sabatelli, M., Belliard, S., Vercelletto, M., Forlani, S., Jornea, L., French, C., Genetic Research Network on, F. F.-A., Prevdemals, Groups, F. T.-E. S.,…Le Ber, I. (2019). Relations between C9orf72 expansion size in blood, age at onset, age at collection and transmission across generations in patients and

presymptomatic carriers. *Neurobiol Aging*, *74*, 234 e231-234 e238. https://doi.org/10.1016/j.neurobiolaging.2018.09.010
Ghasemi, M., & Brown, R. H., Jr. (2018). Genetics of Amyotrophic Lateral Sclerosis. *Cold Spring Harb Perspect Med*, *8*(5). https://doi.org/10.1101/cshperspect.a024125
Gijselinck, I., Van Mossevelde, S., van der Zee, J., Sieben, A., Engelborghs, S., De Bleecker, J., Ivanoiu, A., Deryck, O., Edbauer, D., Zhang, M., Heeman, B., Baumer, V., Van den Broeck, M., Mattheijssens, M., Peeters, K., Rogaeva, E., De Jonghe, P., Cras, P., Martin, J. J.,…Van Broeckhoven, C. (2016). The C9orf72 repeat size correlates with onset age of disease, DNA methylation and transcriptional downregulation of the promoter. *Mol Psychiatry*, *21*(8), 1112-1124. https://doi.org/10.1038/mp.2015.159
Goodman, L. D., Prudencio, M., Kramer, N. J., Martinez-Ramirez, L. F., Srinivasan, A. R., Lan, M., Parisi, M. J., Zhu, Y., Chew, J., Cook, C. N., Berson, A., Gitler, A. D., Petrucelli, L., & Bonini, N. M. (2019). Toxic expanded GGGGCC repeat transcription is mediated by the PAF1 complex in C9orf72-associated FTD. *Nat Neurosci*, *22*(6), 863-874. https://doi.org/10.1038/s41593-019-0396-1
Hales, K. G., Korey, C. A., Larracuente, A. M., & Roberts, D. M. (2015). Genetics on the Fly: A Primer on the Drosophila Model System. *Genetics*, *201*(3), 815-842. https://doi.org/10.1534/genetics.115.183392
Hardiman, O., Al-Chalabi, A., Chio, A., Corr, E. M., Logroscino, G., Robberecht, W., Shaw, P. J., Simmons, Z., & van den Berg, L. H. (2017). Amyotrophic lateral sclerosis. *Nat Rev Dis Primers*, *3*, 17071. https://doi.org/10.1038/nrdp.2017.71
Jeibmann, A., & Paulus, W. (2009). Drosophila melanogaster as a model organism of brain diseases. *Int J Mol Sci*, *10*(2), 407-440. https://doi.org/10.3390/ijms10020407
Jo, M., Lee, S., Jeon, Y. M., Kim, S., Kwon, Y., & Kim, H. J. (2020). The role of TDP-43 propagation in neurodegenerative diseases: integrating insights from clinical and experimental studies. *Exp Mol Med*, *52*(10), 1652-1662. https://doi.org/10.1038/s12276-020-00513-7
Kankel, M. W., Sen, A., Lu, L., Theodorou, M., Dimlich, D. N., McCampbell, A., Henderson, C. E., Shneider, N. A., & Artavanis-Tsakonas, S. (2020). Amyotrophic Lateral Sclerosis Modifiers in Drosophila Reveal the Phospholipase D Pathway as a Potential Therapeutic Target. *Genetics*, *215*(3), 747-766. https://doi.org/10.1534/genetics.119.302985
Kedersha, N., Cho, M. R., Li, W., Yacono, P. W., Chen, S., Gilks, N., Golan, D., E., & Anderson, P. (2000). Dynamic Shuttling of TIA-1 Accompanies the Recruitment of mRNA into Mammalian Stress Granules. *The Journal of Cell Biology*, *151*(6), 1257-1268.
Kim, T., Song, B., & Lee, I. S. (2020). Drosophila Glia: Models for Human Neurodevelopmental and Neurodegenerative Disorders. *Int J Mol Sci*, *21*(14). https://doi.org/10.3390/ijms21144859
Kwiatkowski, T. J., Jr., Bosco, D. A., Leclerc, A. L., Tamrazian, E., Vanderburg, C. R., Russ, C., Davis, A., Gilchrist, J., Kasarskis, E. J., Munsat, T., Valdmanis, P., Rouleau, G. A., Hosler, B. A., Cortelli, P., de Jong, P. J., Yoshinaga, Y., Haines, J. L., Pericak-Vance, M. A., Yan, J.,…Brown, R. H., Jr. (2009). Mutations in the FUS/TLS gene on chromosome 16 cause familial amyotrophic lateral sclerosis. *Science*, *323*(5918), 1205-1208. https://doi.org/10.1126/science.1166066
Lagier-Tourenne, C., Baughn, M., Rigo, F., Sun, S., Liu, P., Li, H. R., Jiang, J., Watt, A. T., Chun, S., Katz, M., Qiu, J., Sun, Y., Ling, S. C., Zhu, Q., Polymenidou, M., Drenner, K.,

Artates, J. W., McAlonis-Downes, M., Markmiller, S.,…Ravits, J. (2013). Targeted degradation of sense and antisense *C9orf72* RNA foci as therapy for ALS and frontotemporal dementia. *PNAS*, *110*(47), E4530-E4539. https://doi.org/10.1073/pnas.1318835110

Li, W. Z., Li, S. L., Zheng, H. Y., Zhang, S. P., & Xue, L. (2012). A broad expression profile of the GMR-GAL4 driver in Drosophila melanogaster. *Genet Mol Res*, *11*(3), 1997-2002. https://doi.org/10.4238/2012.August.6.4

Lloyd, T. E., & Taylor, J. P. (2010). Flightless Flies: *Drosophila* models of neuromuscular disease. *Annals of the New York Academy of Sciences*(1184), e1-20. https://doi.org/10.1111/j.1749-6632.2010.05432.x

Lualdi, M., Casale, F., Rizzone, M. G., Zibetti, M., Monti, C., Colugnat, I., Calvo, A., De Marco, G., Moglia, C., Fuda, G., Comi, C., Chio, A., Lopiano, L., Fasano, M., & Alberio, T. (2023). Shared and Unique Disease Pathways in Amyotrophic Lateral Sclerosis and Parkinson's Disease Unveiled in Peripheral Blood Mononuclear Cells. *ACS Chem Neurosci*, *14*(23), 4240-4251. https://doi.org/10.1021/acschemneuro.3c00629

Mackenzie, I. R., Bigio, E. H., Ince, P. G., Geser, F., Neumann, M., Cairns, N. J., Kwong, L. K., Forman, M. S., Ravits, J., Stewart, H., Eisen, A., McClusky, L., Kretzschmar, H. A., Monoranu, C. M., Highley, J. R., Kirby, J., Siddique, T., Shaw, P. J., Lee, V. M., & Trojanowski, J. Q. (2007). Pathological TDP-43 distinguishes sporadic amyotrophic lateral sclerosis from amyotrophic lateral sclerosis with SOD1 mutations. *Ann Neurol*, *61*(5), 427-434. https://doi.org/10.1002/ana.21147

Mackenzie, I. R., Rademakers, R., & Neumann, M. (2010). TDP-43 and FUS in amyotrophic lateral sclerosis and frontotemporal dementia. *Lancet Neurol*, *9*(10), 995-1007. https://doi.org/10.1016/S1474-4422(10)70195-2

Mahr, A., & Aberle, H. (2006). The expression pattern of the Drosophila vesicular glutamate transporter: a marker protein for motoneurons and glutamatergic centers in the brain. *Gene Expr Patterns*, *6*(3), 299-309. https://doi.org/10.1016/j.modgep.2005.07.006

Manjaly, Z. R., Scott, K. M., Abhinav, K., Wijesekera, L., Ganesalingam, J., Goldstein, L. H., Janssen, A., Dougherty, A., Willey, E., Stanton, B. R., Turner, M. R., Ampong, M. A., Sakel, M., Orrell, R. W., Howard, R., Shaw, C. E., Leigh, P. N., & Al-Chalabi, A. (2010). The sex ratio in amyotrophic lateral sclerosis: A population based study. *Amyotroph Lateral Scler*, *11*(5), 439-442. https://doi.org/10.3109/17482961003610853

Markmiller, S., Soltanieh, S., Server, K. L., Mak, R., Jin, W., Fang, M. Y., Luo, E. C., Krach, F., Yang, D., Sen, A., Fulzele, A., Wozniak, J. M., Gonzalez, D. J., Kankel, M. W., Gao, F. B., Bennett, E. J., Lecuyer, E., & Yeo, G. W. (2018). Context-Dependent and Disease-Specific Diversity in Protein Interactions within Stress Granules. *Cell*, *172*(3), 590-604 e513. https://doi.org/10.1016/j.cell.2017.12.032

Marriott, H., Kabiljo, R., Hunt, G. P., Khleifat, A. A., Jones, A., Troakes, C., Project Min, E. A. L. S. S. C., Target, A. L. S. S. C., Pfaff, A. L., Quinn, J. P., Koks, S., Dobson, R. J., Schwab, P., Al-Chalabi, A., & Iacoangeli, A. (2023). Unsupervised machine learning identifies distinct ALS molecular subtypes in post-mortem motor cortex and blood expression data. *Acta Neuropathol Commun*, *11*(1), 208. https://doi.org/10.1186/s40478-023-01686-8

Masrori, P., & Van Damme, P. (2020). Amyotrophic lateral sclerosis: a clinical review. *Eur J Neurol*, *27*(10), 1918-1929. https://doi.org/10.1111/ene.14393

Mead, R. J., Shan, N., Reiser, H. J., Marshall, F., & Shaw, P. J. (2023). Amyotrophic lateral sclerosis: a neurodegenerative disorder poised for successful therapeutic translation. *Nat Rev Drug Discov*, *22*(3), 185-212. https://doi.org/10.1038/s41573-022-00612-2

Mizielinska, S., Gronke, S., Niccoli, T., Ridler, C. E., Clayton, E. L., Devoy, A., Moens, T., Norona, F. E., Woollacott, I. O. C., Pietrzyk, J., Cleverley, K., Nicoll, A. J., Pickering-Brown, S., Dols, J., Cabecinha, M., Hendrich, O., Fratta, P., Fisher, E. M. C., Partridge, L., & Isaacs, A. M. (2014). C9orf72 repeat expansions cause neurodegeneration in Drosophila through arginine-rich proteins. *Science*, *345*(6201), 1192-1194. https://doi.org/10.1126/science.1256800

Mori, K., Weng, S. M., Arzberger, T., May, S., Rentzsch, K., Kremmer, E., Schmid, B., Kretzschmar, H. A., Cruts, M., Van Broeckhoven, C., Haass, C., & Edbauer, D. (2013). The *C9orf72* GGGGCC Repeat is Translated into Aggregating Dipeptide-Repeat Proteins in FTLD/ALS. *Science*, *339*, 1335-1338. https://doi.org/10.1126/science.1232927

Moron-Oset, J., Fischer, L. K. S., Jaure, N., Zhang, P., Jahn, A. J., Super, T., Pahl, A., Isaacs, A. M., Gronke, S., & Partridge, L. (2023). Repeat length of C9orf72-associated glycine-alanine polypeptides affects their toxicity. *Acta Neuropathol Commun*, *11*(1), 140. https://doi.org/10.1186/s40478-023-01634-6

Park, J. H., Chung, C. G., Park, S. S., Lee, D., Kim, K. M., Jeong, Y., Kim, E. S., Cho, J. H., Jeon, Y. M., Shen, C. J., Kim, H. J., Hwang, D., & Lee, S. B. (2020). Cytosolic calcium regulates cytoplasmic accumulation of TDP-43 through Calpain-A and Importin alpha3. *eLife*, *9*. https://doi.org/10.7554/eLife.60132

Renton, A. E., Majounie, E., Waite, A., Simon-Sanchez, J., Rollinson, S., Gibbs, J. R., Schymick, J. C., Laaksovirta, H., van Swieten, J. C., Myllykangas, L., Kalimo, H., Paetau, A., Abramzon, Y., Remes, A. M., Kaganovich, A., Scholz, S. W., Duckworth, J., Ding, J., Harmer, D. W.,…Traynor, B. J. (2011). A hexanucleotide repeat expansion in C9ORF72 is the cause of chromosome 9p21-linked ALS-FTD. *Neuron*, *72*(2), 257-268. https://doi.org/10.1016/j.neuron.2011.09.010

Riabinina, O., Luginbuhl, D., Marr, E., Liu, S., Wu, M. N., Luo, L., & Potter, C. J. (2015). Improved and expanded Q-system reagents for genetic manipulations. *Nat Methods*, *12*(3), 219-222, 215 p following 222. https://doi.org/10.1038/nmeth.3250

Rosen, D. R., Siddique, T., Patterson, D., Figlewicz, D. A., Sapp, P., Hentati, A., Donaldson, D., Goto, J., O'Regan, J. P., Deng, H.-X., Rahmani, Z., Krizus, A., McKenna-Yasek, D., Cayabyab, A., Gaston, S. M., Berger, R., Tanzi, R. E., Halperin, J. J., Herzfeldt, B.,…Brown, R. H. (1993). Mutations in Cu/Zn superoxide dismutase gene are associated with familial amyotrophic lateral sclerosis [Letters]. *Nature*, *362*, 59-62. https://doi.org/10.1038/362059a0

Sanyal, S. (2009). Genomic mapping and expression patterns of *C380, OK6,* and *D42* enhancer trap lines in the larval nervous system of *Drosophila*. *Gene Expression Patterns*, *9*, 371-380. https://doi.org/10.1016/j.gep.2009.01.002372

Siddique, T., & Ajroud-Driss, S. (2011). Familial amyotrophic lateral sclerosis, a historical perspective. *Acta Myologica*, 117-120.

Smeyers, J., Banchi, E. G., & Latouche, M. (2021). C9ORF72: What It Is, What It Does, and Why It Matters. *Front Cell Neurosci*, *15*, 661447. https://doi.org/10.3389/fncel.2021.661447

van Blitterswijk, M., DeJesus-Hernandez, M., & Rademakers, R. (2012). How do C9ORF72 repeat expansions cause amyotrophic lateral sclerosis and frontotemporal dementia: can

we learn from other noncoding repeat expansion disorders? *Curr Opin Neurol*, *25*(6), 689-700. https://doi.org/10.1097/WCO.0b013e32835a3efb

van der Zee, J., Gijselinck, I., Dillen, L., Van Langenhove, T., Theuns, J., Engelborghs, S., Philtjens, S., Vandenbulcke, M., Sleegers, K., Sieben, A., Baumer, V., Maes, G., Corsmit, E., Borroni, B., Padovani, A., Archetti, S., Perneczky, R., Diehl-Schmid, J., de Mendonca, A.,…European Early-Onset Dementia, C. (2013). A pan-European study of the C9orf72 repeat associated with FTLD: geographic prevalence, genomic instability, and intermediate repeats. *Hum Mutat*, *34*(2), 363-373. https://doi.org/10.1002/humu.22244

Walters, R., Manion, J., & Neely, G. G. (2019). Dissecting Motor Neuron Disease With Drosophila melanogaster. *Front Neurosci*, *13*, 331. https://doi.org/10.3389/fnins.2019.00331

Watanabe, S., Kaneko, K., & Yamanaka, K. (2013). Accelerated disease onset with stabilized familial amyotrophic lateral sclerosis (ALS)-linked mutant TDP-43 proteins. *J Biol Chem*, *288*(5), 3641-3654. https://doi.org/10.1074/jbc.M112.433615

Webster, C. P., Smith, E. F., Bauer, C. S., Moller, A., Hautbergue, G. M., Ferraiuolo, L., Myszczynska, M. A., Higginbottom, A., Walsh, M. J., Whitworth, A. J., Kaspar, B. K., Meyer, K., Shaw, P. J., Grierson, A. J., & De Vos, K. J. (2016). The C9orf72 protein interacts with Rab1a and the ULK1 complex to regulate initiation of autophagy. *EMBO J*, *35*(15), 1656-1676. https://doi.org/10.15252/embj.201694401

Wheeler, J. R., Jain, S., Khong, A., & Parker, R. (2017). Isolation of yeast and mammalian stress granule cores. *Methods*, *126*, 12-17. https://doi.org/10.1016/j.ymeth.2017.04.020

Wheeler, J. R., Matheny, T., Jain, S., Abrisch, R., & Parker, R. (2016). Distinct stages in stress granule assembly and disassembly. *eLife*, *5*. https://doi.org/10.7554/eLife.18413

Winton, M. J., Igaz, L. M., Wong, M. M., Kwong, L. K., Trojanowski, J. Q., & Lee, V. M. (2008). Disturbance of nuclear and cytoplasmic TAR DNA-binding protein (TDP-43) induces disease-like redistribution, sequestration, and aggregate formation. *J Biol Chem*, *283*(19), 13302-13309. https://doi.org/10.1074/jbc.M800342200

Wolozin, B., & Ivanov, P. (2019). Stress granules and neurodegeneration. *Nat Rev Neurosci*, *20*(11), 649-666. https://doi.org/10.1038/s41583-019-0222-5

Wong, P. C., Pardo, C. A., Borchelt, D. R., Lee, M. K., Copeland, N. G., Jenkins, N. A., Sisodia, S. S., Cleveland, D. W., & Price, D. L. (1995). An Adverse Property of a Familial ALS-Linked SOD1 Mutation Causes Motor Neuron Disease Characterized by Vacuolar Degeneration of Mitochondria. *Neuron*, *14*(6), 1105-1116. https://doi.org/10.1016/0896-6273(95)90259-7

Xu, Z., Poldevin, M., Li, X., Li, Y., Shu, L., Nelson, D. L., Li, H., Hales, C., M., Gearing, M., Wingo, T. S., & Jin, P. (2013). Expanded GGGGCC repeat RNA associated with amyotrophic lateral sclerosis and frontotemporal dementia causes neurodegeneration. *PNAS*, *110*(19), 7778-7783. https://doi.org/10.1073/pnas.1219643110

Yun, Y., & Ha, Y. (2020). CRISPR/Cas9-Mediated Gene Correction to Understand ALS. *Int J Mol Sci*, *21*(11). https://doi.org/10.3390/ijms21113801

Zappia, M. P., & Frolov, M. V. (2016). E2F function in muscle growth is necessary and sufficient for viability in Drosophila. *Nat Commun*, *7*, 10509. https://doi.org/10.1038/ncomms10509

Zhang, Y. J., Xu, Y. F., Cook, C., Gendron, T. F., Roettges, P., Link, C. D., Lin, W. L., Tong, J., Castanedes-Casey, M., Ash, P., Gass, J., Rangachari, V., Buratti, E., Baralle, F., Golde,

T. E., Dickson, D. W., & Petrucelli, L. (2009). Aberrant cleavage of TDP-43 enhances aggregation and cellular toxicity. *PNAS*, *106*(18), 7607-7612. https://doi.org/10.1073/pnas.0900688106

Zhou, W., & Xu, R. (2023). Current insights in the molecular genetic pathogenesis of amyotrophic lateral sclerosis. *Front Neurosci*, *17*, 1189470. https://doi.org/10.3389/fnins.2023.1189470

Zu, T., Liu, Y., Bañez-Coronel, M., Reid, T., Pletnikova, O., Lewis, J., Miller, T. M., Harms, M. B., Falchook, A. E., Subramony, S. H., Ostrow, L. W., Rothstein, J. D., Troncoso, J. C., & Ranum, L. P. W. (2013). RAN proteins and RNA foci from antisense transcripts in *C9ORF72* ALS and frontotemporal dementia. *PNAS*, *110*(51), E4968-E4977. https://doi.org/10.1073/pnas.1315438110

Chapter 2 - METHODS

See **Table 2.1** for list of Drosophila lines and their sources. See **Table 2.2** for the details of RNAi vectors and methods of interference. The following solutions and kits were used: phosphate-buffered saline (PBS) (Life Technologies 21300058), RNeasy Mini Kit (Qiagen 74104), RNase-Free DNase Set (Qiagen 79254), 2-Mercaptoethanol (MP Biomedicals 194834), iScript cDNA Synthesis Kit (Bio-Rad 1708891) and SYBR Green Supermix (Bio-Rad 1725270). See **Table 2.3** for list of primers used for gene expression assays. See **Table 2.4** for antibodies used in immunohistochemistry.

Table 2.1. Drosophila Lines Used

Genotype	Source
w;nSyb-Gal4/CyO-YFP;;	Made by Jonah Boardman; generated from stock by Julia Cordero, University of Glasgow
w; UAS-(G4C2)49;;	Nancy Bonini, University of Pennsylvania
w[1118];;	Well Genetics
y[1]v[1];;P{y[+7.7]v[+t1.8]=TRiP.HMS00038}attP2(UAS-otu-RNAi)	BDSC #34065
y[1]sc[*]v[1]sev[21];;P{y[+t7.7]v[+t1.8]=TRiP.HMS00597}attP2(UAS-Hrb27C-RNAi)	BDSC #33716
w/yv;;P{y[+t7.7]v[+t1.8]=TRiP.HMS00184}attP2}(UAS-Tudor-SN-RNAi)/TM6b, tb	Made from BDSC #34865
w[1118];; P{w[+mC]=UAS-lacZ.NZ}J312	BDSC #3956
y[1]sc[*]v[1]sev[21];; P{y[+t7.7]v[+t1.8]=TRiP.HMS00182}attP2(UAS-mle-RNAi)	BDSC #34864
w; OK371-Gal4; UAS-dTDP-43[N493D]/TM6b, tub-Gal80	Mark Kankel
w; OK371-Gal4;;	Robert Reenan, Brown University
OreR	Unknown
w;OK6-Gal4, UAS-G4C2(30X)-GFP/CyO, Tub-Gal80ts; +/TM6b, tb	Mark Kankel
w;OK6-Gal4;;	Aberle et al., 2002
y[1]v[1];;P{y[+t7.7]v[+t1.8]=TRiP.JF02616}attP2(UAS-CanB-RNAi)	BDSC #27307
y[1]sc[*]v[1]sev[21];;P{y[+t7.7]v[+t1.8]=TRiP.HMS01318}attP2(UAS-Cam-RNAi)	BDSC #34609

y[1]sc[*]v[1]sev[21];;P{y[+t7.7]v[+t1.8]=TRiP.HMC04134}attP2(UAS-Pkc53E-RNAi)	BDSC #55864
y[1]sc[*]v[1]sev[21];;P{y[+t7.7]v[+t1.8]=TRiP.HMC02411}(UAS-NFAT-RNAi)	BDSC #51422
y[1]v[1];;P{y[+t7.7]v[+t1.8]=TRiP.HM05194}attP2(UAS-TBPH-RNAi)	BDSC #29517
w;;tubulin-Gal4/Tm6b	Unknown
yw;;GMR-p53(R155H/T(2;3), Cy, Tb, Hu	BDSC#8428

Table 2.2. RNAi Reagents

RNAi	**Source**	**Vector**	**Method of Interference**
otu-RNAi	BDSC #34065	Valium 20	Short hairpin RNA
Tudor-SN-RNAi	BDSC #34865	Valium 20	Short hairpin RNA
Hrb27C-RNAi	BDSC #33716	Valium 20	Short hairpin RNA
mle-RNAi	BDSC #34864	Valium 20	Short hairpin RNA
TBPH-RNAi	BDSC #29517	Valium 10	Long double-stranded RNA
CanB-RNAi	BDSC #27307	Valium 10	Long double-stranded RNA
Cam-RNAi	BDSC #34609	Valium 20	Short hairpin RNA
Pkc53E-RNAi	BDSC #55864	Valium 20	Short hairpin RNA
NFAT-RNAi	BDSC #51422	Valium 20	Short hairpin RNA

Table 2.3. qPCR Primer Sequences

Gene	**Forward**	**Reverse**	**Source**
RP49	AGC ATA CAG GCC CAA GAT CG	TGT TGT CGA TAC CCT TGG GC	Invitrogen
TBPH	TTC TGT CCA CAC TGC AAG CTC	AGA CGC AAA AGT AAG CGT ACT C	IDT
otu	TGC CCA AGT ATG CCG GTA AG	ATA GCA ATT GTC CAC GGG CA	IDT
Hrb27C	ACA TGC CAC CTA ACT CTG CC	TTG AGC ACG CGA GTA CAT GT	IDT
Tudor-SN	TTA TTC GCG CAA CTA AGG GTG	GTC CTT GGT CTC GTC TCC G	IDT

Table 2.4 Antibodies Used

Antibody/Stain	Catalog Number	Source
Anti-TBPH (guinea pig)	n/a	Artavanis-Tsakonas Lab, Harvard University (Ho et al., 2024)
Anti-Eve (rat)	7E8A10	DSHB
488 goat anti-guinea pig	A-11073	Invitrogen
555 goat anti-rat	A-21434	Invitrogen

2.1 Lifespan Assays

For all lifespan experiments, approximately two male and three virgin female parents were combined in glass vials containing standard cornmeal/sugar/inactive brewer's yeast/agar food, supplemented with active dry yeast. Crosses were kept at 25°C on a 12hr light:12hr dark cycle, and brooded every 48 hours. Crosses were set up in triplicate. For all experiments, progeny were collected every 24 hours up to 6 days after first eclosion and scored on CO_2. Lifespans were conducted on progeny kept in vials of up to 10 flies of the same genotypes, sex, and eclosion date with viability scored every 24 hours. Vials were incubated horizontally at 25°C and brooded every 4 days.

2.2 Climbing Assay

Biological replicates from the experiments reported in Figure 3.1 were used for the measurement of climbing velocities depicted in Figure 3.2. Female progeny that eclosed over a single 24-hour period were collected and sorted on CO_2. Flies were kept overnight at 25°C to recover from CO_2 before the first climbing trial was performed the following day. Flies were climbed once a day on

days 1, 3, 5, and 6 after eclosion. Beginning on day 7, an additional timepoint was introduced in the afternoon. Light was controlled for the experiment with the overhead lights in the room kept off. Vials of flies were kept horizontally at 25°C with up to 5 flies per genotype and were brooded every 4 days. Flies were maintained on standard food of cornmeal/sugar/inactive brewer's yeast/agar food supplemented with active dry yeast. Videos collected were analyzed through the FreeClimber software with Python. Cohort climbing kinematics are plotted over a ten second time period in conjunction with the mean y-position in centimeters. The slope of the line for period of climbing is calculated utilizing the distance traveled (cm) over time (s). The slope is representative of the climbing velocity (cm/s). See Spierer et al. for additional information regarding the process of recording videos and analysis via the software, FreeClimber (Spierer et al., 2021).

2.3 Adult Viability and Eclosion Assay

For all eclosion experiments, progeny that eclosed were included in a lifespan assay. Male and virgin female parents were combined in glass vials containing cornmeal/sugar/inactivate brewer's yeast/agar food, supplemented with active dry yeast. Progeny were collected every 24 hours and scored on CO_2. After six days of eclosion, uneclosed pupae were scored. Crosses were kept at 25°C and brooded every 48 hours. After collection, progeny was kept horizontally at 25°C. Progeny were scored for new deaths every 24 hours and brooded every 4 days.

2.4 Gene Expression qPCR Assays

Male and virgin female parents were combined in vials containing cornmeal/sugar/inactive brewer's yeast/agar food, supplemented with active dry yeast. For all *OK371>TBPH[N493D]*

qPCR experiments depicted, third instar wandering larvae were collected from the surface of the vial and collected for dissection. Larvae were collected with forceps and washed in a glass well containing 50µl 1X phosphate-buffered saline (PBS) on wet ice, and transferred to a silicone plate with 50µl of 1X PBS once ready for dissection. Larvae were cut perpendicular to the midline at the posterior end. The anterior portion of the larvae was then pushed inwards to invert the body and expose the brain and VNC. All additional tissues were removed and the VNC was collected for each organism. Dissections were added to a 1.5 mL centrifuge tube kept on wet ice. After all dissections per genotype were completed, dissections were flash frozen and moved to long-term storage at -80°C. After all collections were completed, samples were thawed on ice and homogenized. RNA was isolated using the Qiagen RNeasy Mini Kit and treated with the RNase-Free DNase set.

For all *tubulin-Gal4>SG-RNAi* qPCR experiments depicted, third instar wandering larvae were collected from the surface of the vial and collected for dissection. Larvae were collected with forceps and washed in a glass well containing 50µl 1X phosphate-buffered saline (PBS) on wet ice. Whole, third instar wandering larvae were added to a 1.5 mL centrifuge tube kept on wet ice. Samples were flash frozen and moved to long-term storage at -80°C. After all collections were completed, samples were thawed on ice and homogenized. RNA was isolated using the Qiagen RNeasy Mini Kit and treated with the RNase-Free DNase set.

2.5 VNC Dissections and Immunofluorescence

Male and virgin female parents were combined in vials containing standard cornmeal/sugar/inactive brewer's yeast/agar food, supplemented with active dry yeast. Crosses were kept at 25 °C and were brooded every 4 days. For all genotypes depicted in Figure 3.5,

third instar wandering larvae were collected for dissection. For *OK371>TBPH[N493D]/Hrb27C-RNAi* in Figure A.12, larvae were collected from the surface of the food. Larvae were collected with forceps, quickly washed in a glass well containing 100µl of 1X PBS on wet ice, and then transferred to a silicone plate with 50µl 1X PBS. Larvae were cut perpendicular to the midline at the posterior end. The anterior portion of the larvae was then pushed inwards to invert the body and expose the brain and VNC. All additional tissues were removed and the VNC was collected for each organism. Dissections were then fixed in 25µl of 4% paraformaldehyde (PFA) for 17 minutes, and then washed twice in the glass wells with 100µl of 0.3% PBS with Triton (PBT), and then transferred to a clean well (1 per genotype) containing 100µl of 0.3% PBT.

All samples were kept in 0.3% PBT on a shaker at 4°C until all dissections were completed. Dissections were then twice washed in 0.3% PBT. Dissections were blocked in 100µl of 1:25 normal goat serum (NGS) in 0.3% PBT for 1 hour on a shaker at RT. Blocking solution was then removed and 100µl of primary antibody solution (1:1000 anti-TBPH, 1:500 anti-elav, 1:100 NGS, 0.3% PBT) was then added and samples were left on shaker at 4°C overnight. The following day, the primary antibody solution was removed, and dissections were washed quickly 3X in 100µl of 0.3% PBT. Samples were then washed in 0.3% PBT on a shaker kept at RT for successive washing timepoints (10 minutes, 20 minutes, 30 minutes (x2), 20 minutes, 10 minutes). 100µl of secondary antibody solution was then added (1:200 goat anti-guinea pig 488, 1:200 goat anti-rat 555, 1:100 NGS, 0.3% PBT). Samples were incubated in secondary antibody for 2 hours at RT on a shaker. After incubation, samples were washed 3x quickly with 0.3% PBT and then washed in 0.3% PBT on a shaker at RT for the following incubation times (10 minutes, 20 minutes, 30 minutes (x2), 20 minutes, 10 minutes). Samples were then washed 3x quickly in

0.3% PBT and prepared for mounting. Samples were mounted on a glass slide in 30µl of 80% glycerol with 0.5% N-propyl-gallate. Brain lobes and imaginal discs were kept on when mounting the VNC. Coverslip was secured with nail polish and stored at 4°C before imaging on Zeiss LSM800 confocal microscope. Master gain was held constant for all genotypes: 580V for the 488nm channel and 500V for the 555nm channel. N:C ratios were quantified by dividing cytoplasmic total fluorescence, normalized to area, by nuclear total fluorescence, normalized to area and quantified in FIJI.

2.6 References

Ho, D. M., Shaban, M., Mahmood, F., Ganguly, P., Todeschini, L., Van Vactor, D., & Artavanis-Tsakonas, S. (2024). cAMP/PKA signaling regulates TDP-43 aggregation and mislocalization. *Proc Natl Acad Sci U S A*, *121*(24), e2400732121. https://doi.org/10.1073/pnas.2400732121

Spierer, A. N., Yoon, D., Zhu, C. T., & Rand, D. M. (2021). FreeClimber: automated quantification of climbing performance in Drosophila. *J Exp Biol*, *224*(Pt 2). https://doi.org/10.1242/jeb.229377

Chapter 3 – RESULTS

3.1 Introduction

Stress granules (SGs) are cytoplasmic aggregations that are primarily composed of proteins and untranslated mRNAs that form under cellular stress (Fan & Leung, 2016; Kankel et al., 2020; Marcelo et al., 2021; Markmiller et al., 2018; Wolozin & Ivanov, 2019). While the exact function of stress granules is unknown, they are generally accepted to be cytoprotective (Wolozin & Ivanov, 2019). Markmiller et al., (2018) identified 150 novel proteins that co-localize to stress granules utilizing APEX proximity labeling against anti-G3BP1, a core component of stress granules. Approximately 20% of the SG-associated protein population was also identified to be dependent on the source of stress and/or the cell type (Markmiller et al., 2018).

Four of the genes that were identified were *otu* (*hOTUD4*), *Hrb27C* (*hDAZAP1*)*, Tudor-SN* (*hSND1*), and *mle* (*hDHX9*). Each of these genes span an array of molecular functions from deubiqitination (*otu*) and dorsalization of the *Drosophila* embryo (*otu, Hrb27C*) to regulation of lipid storage, transcriptional co-activation, regulation of splicing and RISC assembly (*Hrb27C, Tudor-SN, mle*) (Aktas et al., 2017; Bhogal et al., 2020; Cugusi et al., 2015; Das et al., 2019; Finger et al., 2023; Gao et al., 2023; Goodrich et al., 2004; Gutierrez-Beltran et al., 2016; Johnson et al., 2020; Morra et al., 2011; Navarro-Imaz et al., 2020; Reenan et al., 2000). For this thesis, I tested whether knockdown of four SG-associated proteins can rescue *Drosophila* models of ALS through a variety of molecular and functional assays. In the previous study conducted, these four SG-associated proteins were successful in a stress-dependent environment in

mammalian culture and in an ALS adult *Drosophila* eye screen. Of the four, three are RNA binding proteins and one (*otu*) is a deubiquitinase.

In these previous studies, knockdown of the four SG-associated genes using RNAi silencing rescued degeneration of photoreceptors observed in a *hTDP-43*^{M337V} and a *FUS*^{R521C} *Drosophila* eye screen (Markmiller et al., 2018). Adult viability varied across ALS models tested and drivers utilized. Overexpressing 49X G4C2 HRE with an *nSyb-Gal4* driver resulted in a significantly decreased median lifespan compared to WT adults in females. Males did not eclose. This HRE in females also resulted in reduced climbing velocity. An overexpression of 30X G4C2 HRE with an *OK6-Gal4* driver resulted in a failure of progeny to eclose from the pupal case, unable to reach adult stage. An overexpression of *TBPH[N493D]* with an *OK371-Gal4* driver resulted in a failure to eclose from the pupal case as well. This overexpression with *OK371-Gal4* also results in localization of TBPH in the cytoplasm of motor neurons as opposed to its WT position in the nucleus. Each of the genetic modifiers measured in these experiments were modifiers in at least one of the assays tested.

3.2 Knockdown of *mle, Tudor-SN, and Hrb27C* extends lifespan of nSyb>G4C2(49X) model

For our models, we define adult viability as the ability to survive to adulthood via eclosion from the pupal case. In these experiments, we utilize a *UAS-G4C2(49X)* line created by the Bonini lab (Goodman et al., 2019). This line closely resembles the RAN translation observed in patients as it does not include an AUG start codon prior to the expressed repeats. In our *nSyb>G4C2(49X)* model, we are unable to determine whether progeny that did not eclose from the pupal case have the *nSyb-Gal4* driver due to the *CyO* balancer that is unable to be detected prior to adulthood. As the *nSyb-Gal4/CyO* construct is on the second chromosome as well as *UAS-G4C2(49X)*, we are confident that all progeny that eclose without curly wings will be

constructed as *nSyb-Gal4>UAS-G4C2(49X).* RNAi constructs for each of our SG-associated genes were crossed to our *nSyb>G4C2(49X)* model to assess lifespan extension in males and females. In the *nSyb>G4C2(49X)* disease model, male progeny do not eclose and female progeny have a median survival (days after eclosion) of 11 days (Figure 3.1). Our negative control was *UAS-lacZ*, which should not have any effect on the model as lacZ is not native to *Drosophila*. Knockdown of *otu* had a similar lifespan to the disease model in females, but was able to produce two males. Expression of *UAS-Tudor-SN-RNAi, UAS-Hrb27C-RNAi, and UAS-mle-RNAi* extended the lifespan of the disease model with median lifespans of 16, 24, and 37 days respectively (Figure 3.1).

Knockdown of *mle* was particularly successful in the male disease model as well, with a median lifespan of 32 days. With the other three RNAi knockdowns all yielding less than 10 males, the *UAS-mle-RNAi* yielded 49 males. The significance of these comparisons was verified with a Mantel-Cox Test. In addition, RNAi validation was completed with qPCR for the RNAi's against *otu, Hrb27C,* and *Tudor-SN*. All crosses were set up utilizing a tubulin-Gal4 driver, which expresses in all cells. qPCR validation of *mle-RNAi* is ongoing (Figure A.11).

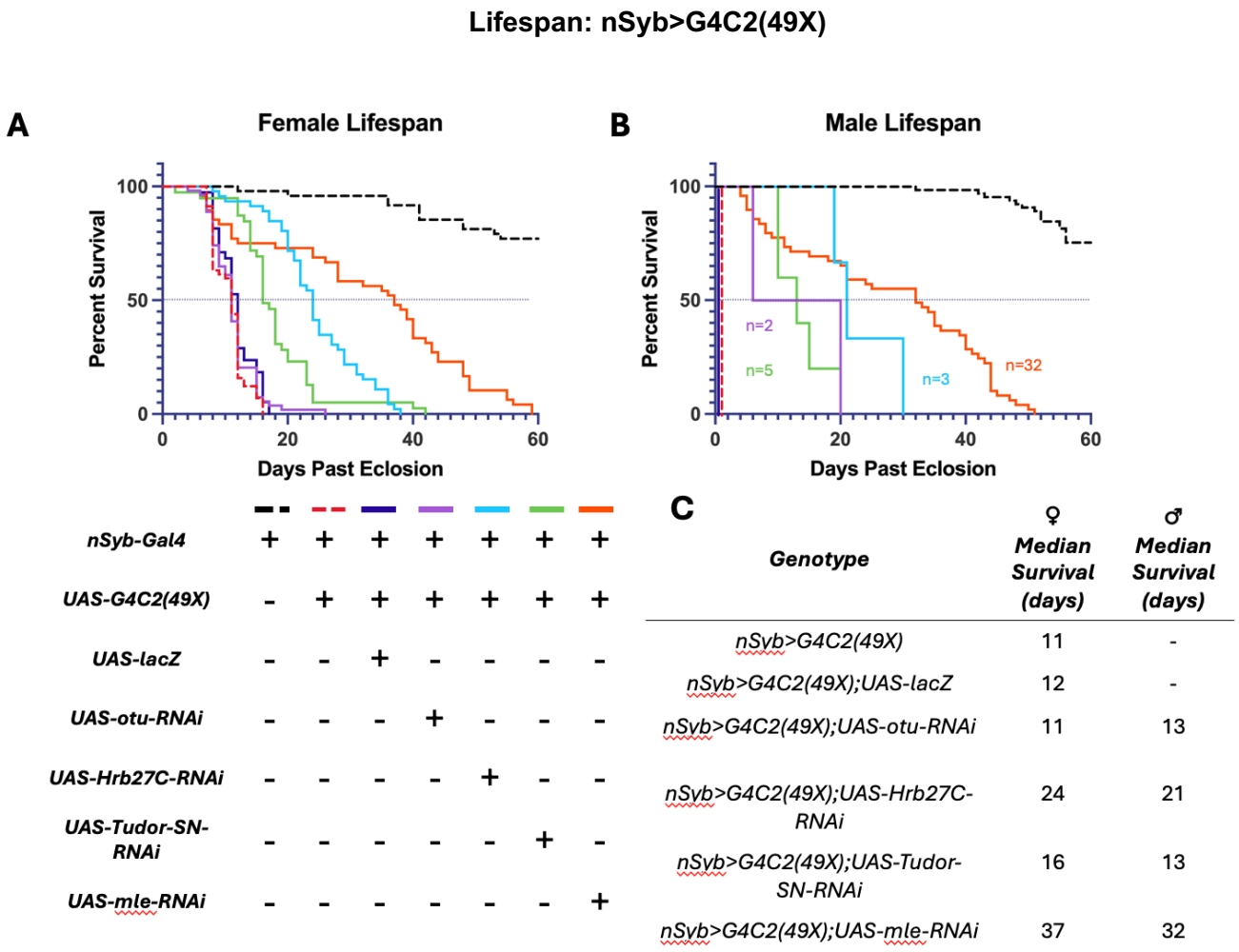

C

Genotype	♀ Median Survival (days)	♂ Median Survival (days)
nSyb>G4C2(49X)	11	-
nSyb>G4C2(49X);UAS-lacZ	12	-
nSyb>G4C2(49X);UAS-otu-RNAi	11	13
nSyb>G4C2(49X);UAS-Hrb27C-RNAi	24	21
nSyb>G4C2(49X);UAS-Tudor-SN-RNAi	16	13
nSyb>G4C2(49X);UAS-mle-RNAi	37	32

Figure 3.1: Lifespan assay of nSyb>G4C2(49X) Lifespans are represented by Kaplan-Meier curves. *nSyb-Gal4* (♀ n = 48, ♂n=65). *nSyb-Gal4>UAS-G4C2(49X)* (♀ n=57). *nSyb-Gal4>UAS-G4C2(49X);UAS-otu-RNAi* (♀ n=54, ♂n=2). *nSyb-Gal4>UAS-G4C2(49X);UAS-Hrb27C-RNAi* (♀ n=46, ♂n=3). *nSyb-Gal4>UAS-G4C2(49X);UAS-Tudor-SN-RNAi* (♀ n=39, ♂n=5). *nSyb-Gal4>UAS-G4C2(49X);UAS-mle-RNAi* (♀ n=48, ♂n=32). *nSyb-Gal4>UAS-G4C2(49X);UAS-lacZ* (♀ n=38). Mantel-Cox tests were performed on complete lifespan curves. All comparisons between models ($p<0.0001$).

3.3 Knockdown of *mle, Hrb27C* rescue climbing velocity of nSyb>G4C2(49X) model

A significant motivation to utilize the *nSyb-Gal4* pan-neuronal driver, is that it permits the observation of adult phenotypes in the *nSyb>G4C2(49X)* model. Due to the lifespan extension with knockdown of *mle*, *Hrb27C*, and *Tudor-SN*, we asked whether knockdown of

each of our SG-associated genes could rescue the climbing defect observed in the *nSyb>G4C2(49X)* model. Flies experience negative geotaxis, therefore a common motor assay to assess this behavior is a rapid iterative negative geotaxis assay (RING) (Gargano et al., 2005) . We refer to this as a climbing assay. Utilizing a climbing apparatus and the FreeClimber software written by Spierer et al., we quantified the average climbing velocity of our ALS models throughout their lifespans (Spierer et al., 2021). Each genotype was climbed in vials of five flies each. Flies were climbed once a day on days 1, 3, 5, and 6 of their lifespans. Beginning on day 7, the flies were climbed twice a day with approximately 6 hours in between the AM and PM climbs. Due to the lethality of the *nSyb*-driven HRE in males, only females were studied in this experiment.

We observe a progressive decline in climbing velocity over the course of the lifespan of the *nSyb>G4C2(49X)* flies (Figure 3.2-A). This is also observed across all genotypes, including *nSyb>+*. To assess climbing velocities across genotypes, unpaired t-tests were run at each timepoint to compare differences in velocities across the lifespan (Tables A.5-A.10). In order to evaluate degeneration of climbing ability, climbing velocities were compared from the timepoints of one day after eclosion through the morning climb 10 days after eclosion as well as the period of time from the afternoon climb 10 days after eclosion to the end of lifespan. In addition to the extension in lifespan observed, a knockdown of *Hrb27C* and *mle* were able to slow the motor decline of the ALS model in females (Figure 3.2-C,E) with significant differences in climbing velocities observed past day 10. Importantly, knockdown of *mle* was significantly improved in the earlier stages of the experiment as well (Figure 3.2-E). While *Tudor-SN* knockdown does extend the lifespan of the model, there is a slight rescue of the climbing velocity once approximately 50% of the disease model flies have died (Figure 3.2-D).

Interestingly, there was a strong improvement of climbing velocity in the *nSyb>G4C2(49);lacZ* model in earlier stages of the experiment, however due to issues with collecting progeny for this cross, the starting number of flies for this genotype was much lower relative to the other genotypes assessed (Figure 3.2-F).

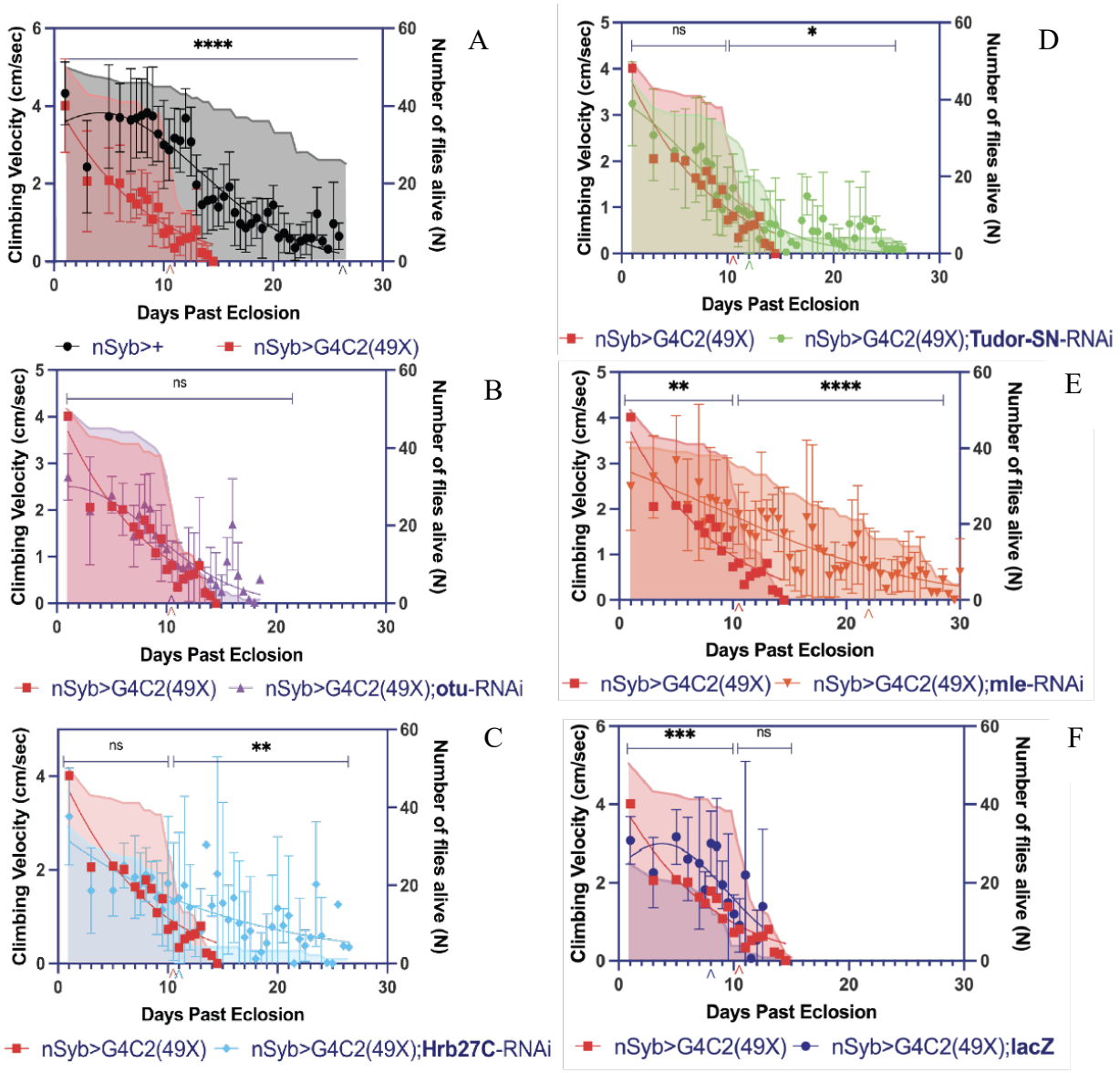

Figure 3.2: Climbing assay of nSyb>G4C2(49X) females.
Means with error bars are presented of technical replicates of vials consisting of ~5 females per vial. Flies were climbed once a day on Days 1, 3, 5, and 6 after eclosion. Flies were climbed twice a day beginning on Day 7. Climbing velocities (cm/sec) represented on left y-axis. All flies

raised at 25ºC. Starting number of flies is n≥35 for all genotypes aside from nSyb>G4C2(49X);lacZ with a starting quantity of n≥25. Solid lines represent Gaussian non-linear regressions. Small ^ symbols on X-axis represent point where more than 50% of progeny in experiment have died. Shaded histograms represent total number of flies alive throughout climbing assay and the approximate number of flies is represented on the right y-axis. An ordinary two-way ANOVA (*p≤0.5, **p≤0.01, ***p≤0.001, ****p≤0.0001) was performed on results from timepoints of day 1 through day 10 and from days 10.5 through end of experimental timepoints for that comparison. Software for data collection and analysis can be found in Spierer et al., 2021.

3.4 Knockdown of SG-associated genes rescues eclosion defect in OK6>G4C2(30X) ALS model

The second G4C2 line that is utilized in this thesis was designed by the Jin lab at Emory University. The UAS-G4C2(30X) line consists of a tandem of two stretches of 15 G4C2 repeats followed by an EGFP tag past the translation start site (Xu et al., 2013). It also includes an AUG start codon unlike the 49X model used in sections 3.2 and 3.3. In the following experiment, the 30X repeat model was used in conjunction with an *OK6-Gal4* driver. *OK6-Gal4* drives the *UAS-G4C2(30X)* expansion in motor neurons only. In this model, we observe a failure of the disease model (*OK6>G4C2(30X)*) to eclose from the pupal case. This indicates a failure of the model to reach adulthood as well as a motor defect in the model as they do reach pharate stage.

RNAi's for each of our genes of interest were used against the *OK6>G4C2(30X)* model. Knockdown of each of our SG-associated genes resulted in not only a rescue of the eclosion defect, but also a significant extension to lifespan. It is important to note that due to issues with setting up the genetic crosses for this experiment utilizing the *UAS-Hrb27C-RNAi* line, the *n* for *OK6>G4C2(30X);Hrb27C-RNAi* is significantly lower compared to the other RNAi's tested and a repeat of these experiments is ongoing. In females, the lowest median lifespan is with *Hrb27C-RNAi* at 47 days but knockdown of *Tudor-SN* is 61 days (Figure 3.4-A). Aside from knockdown of *Hrb27C* there is a great difference between knockdown of *Tudor-SN* between males and

females, with females having a much larger extension in lifespan compared to males, 61 days compared to 46 days (Figure 3.4-A, B).

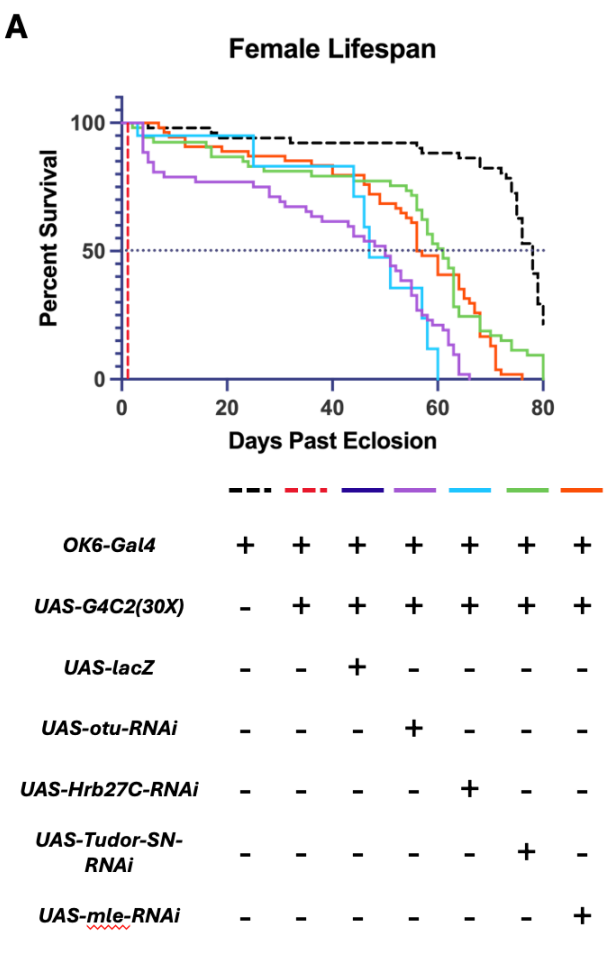

C

Genotype	♀ Median Survival	♂ Median Survival
OK6>G4C2(30X)	-	-
OK6>G4C2(30X);UAS-lacZ	-	-
OK6>G4C2(30X);UAS-otu-RNAi	50	50
OK6>G4C2(30X);UAS-Hrb27C-RNAi	47	28
OK6>G4C2(30X);UAS-Tudor-SN-RNAi	61	46
OK6>G4C2(30X);UAS-mle-RNAi	56.5	60
OK6>+	78	68

Figure 3.3: Lifespan Assay of OK6>G4C2(30X). Lifespans are represented by Kaplan-Meier curves. *OK6-Gal4* (♀n = 51, ♂n=51). *OK6-Gal4>UAS-G4C2(30X);UAS-otu-RNAi* (♀n=52, ♂n=50). *OK6-Gal4>UAS-G4C2(30X);UAS-Hrb27C-RNAi* (♀n=20, ♂n=9). *OK6-Gal4>UAS-G4C2(30X);UAS-Tudor-SN-RNAi* (♀n=53, ♂n=50). *OK6-Gal4>UAS-G4C2(30X);UAS-mle-RNAi* (♀n=54, ♂n=50). Mantel-Cox tests were performed on complete lifespan curves. All comparisons between models ($p<0.0001$).

3.5 Knockdown of *otu*, *Hrb27C*, and *mle* rescue eclosion defect in *OK371>TBPH[N493D]* ALS model

With rescues observed in the *C9orf72*-ALS experiments, our next aim was to determine if similar rescues would be observed in a different model of ALS. In the following experiments, we

utilize a *UAS-TBPH[N493D]* line that uses an equivalent mutation to the patient allele *TARDBP[N378D]* (Ho et al., 2024; Markmiller et al., 2018). This mutation when driven with *OK371-Gal4*, results in a failure for adults to eclose from the pupal case. While not a factor in the *nSyb>G4C2(49X)* model viability and climbing assays, knockdown of *otu* significantly suppresses the *OK371>TBPH[N493D]* eclosion defect. Knockdown of *Hrb27C* and *mle* also results in eclosion from the pupal case.

From here, we collected progeny that did eclose and separated males and females for a lifespan experiment. Knockdown of *otu* and *Hrb27C* resulted in similar median lifespans for males and females. However, there was a great difference in lifespan with knockdown of *mle* as females had a median lifespan of 14 days whereas males had a median lifespan of 7 days (Figure 3.4). While *Tudor-SN* silencing rescued both models of C9-ALS, there was no effect in the TDP-43 disease model. As we are utilizing a mutation to the *Drosophila* gene *TBPH*, we also quantified *TBPH* expression in the disease model as well as with the *otu-RNAi* rescue. We observe an increase in *TBPH* expression in the disease model relative to WT but with a slight decrease in expression with the addition of *otu-RNAi*. However, the reduced expression is not as severe as is seen with a *TBPH-RNAi* in the *TBPH* disease model background. These qPCR results can be found in the Appendix (Figure A.11-A, B).

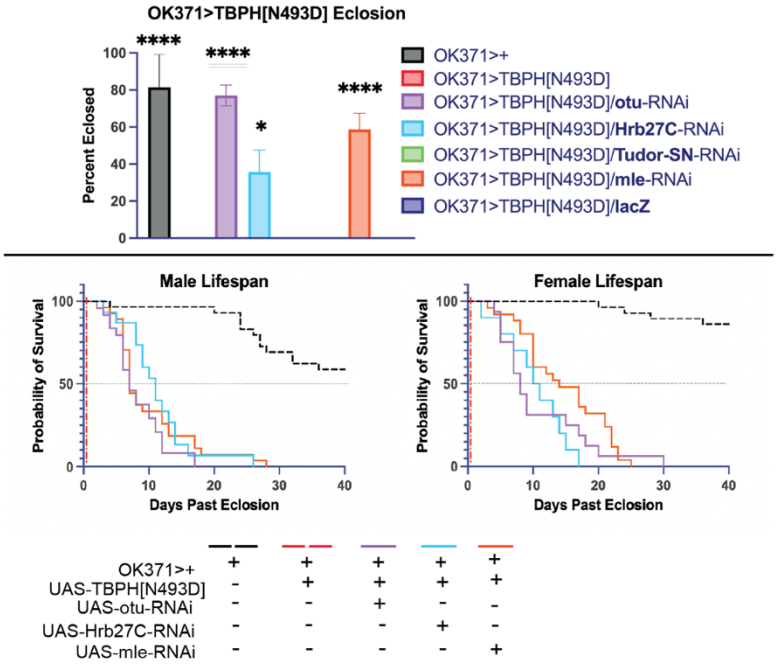

Genotype	♀ Median Survival (days)	♂ Median Survival (days)
OK371>TBPH[N493D]	-	-
OK371>TBPH[N493D]/UAS-lacZ	-	-
OK371>TBPH[N493D]/UAS-otu-RNAi	8	7
OK371>TBPH[N493D]/UAS-Hrb27C-RNAi	10.5	11
OK371>TBPH[N493D]/UAS-mle-RNAi	14	7

Figure 3.4: Eclosion and Lifespan Assays in *OK371>TBPH[N493D]* model with SG-RNAi's Lifespans are represented by Kaplan-Meier curves. *OK371>+* (♀n = 28, ♂n=29). *OK371>TBPH[N493D]/otu-RNAi* (♀n=16, ♂n=24). *OK371>TBPH[N493D]/Hrb27C-RNAi* (♀n=10, ♂n=15). *OK371>TBPH[N493D]/mle-RNAi* (♀n=25, ♂n=27). All flies raised at 25ºC. Mantel-Cox tests were performed on complete lifespan curves. Eclosion statistical testing: one-way ANOVA, *p<0.05, ****p<0.0001. Lifespan statistical testing: all comparisons between models for lifespan Mantel-Cox test (p<0.0001).

3.6 RNAi silencing of *Tudor-SN* relocalizes TBPH from the cytoplasm to the nucleus in *OK371>TBPH[N493D]* ALS model

A common pathological hallmark of TDP-43 ALS is accumulation of TDP-43 aggregates in the cytoplasm of the cell. As knockdown of stress granule-associated genes resulted in an eclosion and lifespan rescue of the *OK371>TBPH[N493D]* model, we aimed to study a potential molecular basis for the results observed in section 3.5. We assessed dorsal midline motor neurons *of OK371>TBPH[N493D]* in 3rd instar wandering larvae and visualized TBPH using an anti-TBPH antibody described in Ho et al., (Ho et al., 2024).

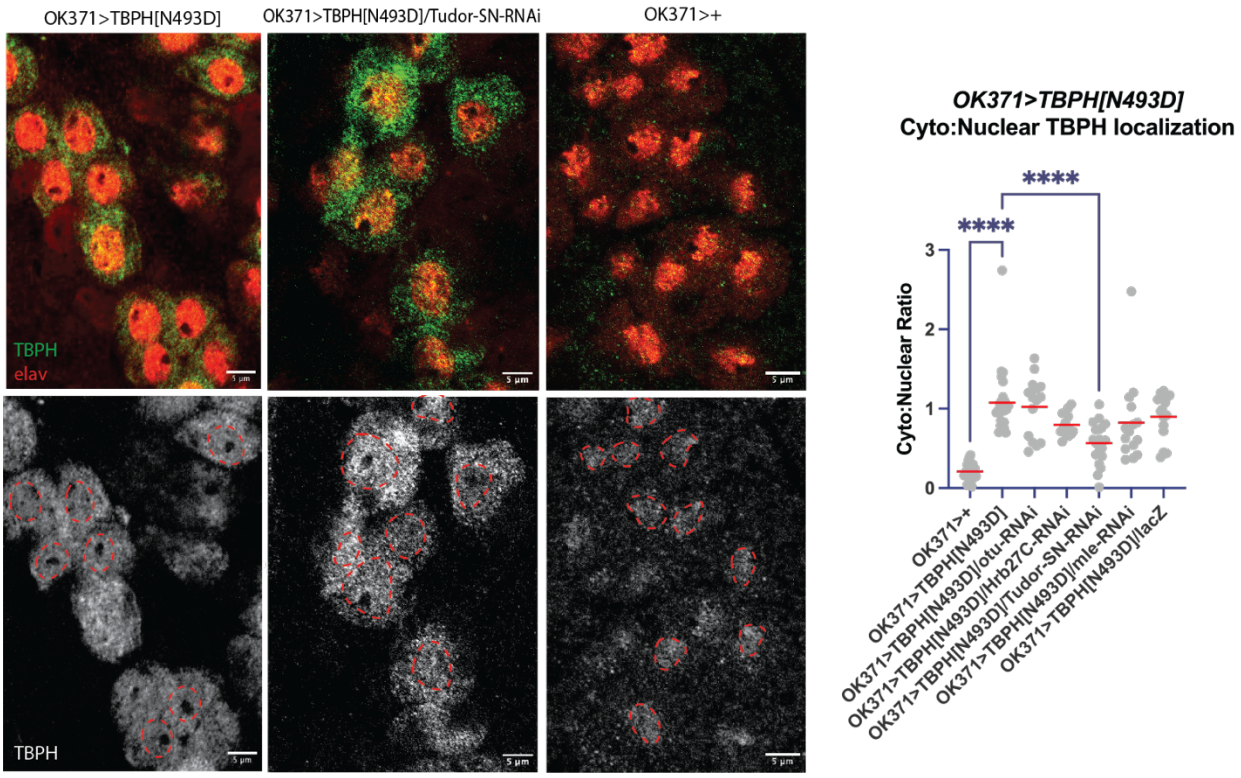

Figure 3.5: Cellular TBPH localization in *OK371>TBPH[N493D]* Midline Dorsal Motor Neurons Quantification of cytoplasmic to nuclear ratio of TBPH in A4 motor neurons. Quantifications were performed on unadjusted images of single slice in Z-stack. All images are 0.25-micron slices taken at 63X oil. Both channels were adjusted for brightness and contrast. Dotted red lines in bottom panel represent nuclear boundary. Ratios were quantified by dividing corrected cytoplasmic total fluorescence, normalized to area, by corrected nuclear total fluorescence, normalized to area. Quantification performed in at least three biological replicates per genotype. Five cells quantified per each biological replicate. One-way ANOVA was performed with comparison to *OK371>TBPH[N493D]*. ****p<0.0001.

Endogenous TBPH is detectable in nuclei of neurons in the larval VNC of the *OK371>+* control (Figure 3.5). The overall level of TBPH is considerably higher in motor neurons of the ALS model *OK371>TBPH[N493D]* given that the *UAS-TBPH[N493D]* transgene is being overexpressed. Importantly, TBPH staining is at high levels in the cytoplasm, as well as the nuclei of motor neurons, with an average cytoplasmic:nuclear ratio of 1.08 in fifteen motor neurons. Knockdown of *otu, Hrb27C,* and *mle* resulted in similar, cytoplasmic localization of TBPH. Upon knockdown of *Tudor-SN*, we see greater expression of TBPH in the nucleus relative to the cytoplasm (Figure 3.5). We then quantified the cytoplasmic-to-nuclear localization

ration in the A4 segment of the *Drosophila* ventral nerve cord (VNC) (Figure 3.5). We observe a significantly lower ratio of TBPH mis-localization relative to the other RNAi's studied. Interestingly, while otu, Hrb27C and mle RNAi's suppressed defects associated with ALS in adult-stage functional assays, such as eclosion and lifespan, we did not see that knockdown of these genes altered mislocalization of TBPH[N493D] evident in larval motor neurons.

3.7 Silencing of Ca^{2+} pathways rescues eclosion defect of *OK371>TBPH[N493D]* model

TBPH along with its human ortholog TDP-43 is known to localize to the nucleus of the cell under non-pathological conditions. TDP-43 has previously been shown to shuttle between the nucleus and the cytoplasm. Levels of cytosolic calcium have been shown to direct this shuttling activity that influences TDP-43 localization. Increases in cytosolic calcium levels reduces TDP-43 aggregation (Park et al., 2020). In order to gain greater understanding for what is potentially factoring into the re-localization of TBPH observed with a knockdown of *Tudor-SN,* we tested RNAi's described in Park et al., 2020 for an effect on TBPH distribution in our model. We selected four lines that had either resulted in TDP-43 re-localization to the nucleus under pathological conditions, *or* that failed to alleviate aggregation of TDP-43 in the cytoplasm in a murine TDP-43 overexpression model. These genes of interest are *calmodulin, NFAT, Pkc53E,* and *CanB*. We first investigated whether any of these genes could rescue the eclosion defect observed in our *OK371>TBPH[N493D]* model as well as whether any rescues observed corroborates with the TBPH localization data within Park et al.

We observed a significant rescue in eclosion when knocking down three of the four selected calcium level modifiers (*CanB, Pkc53E,* and *NFAT*). Park et al. observed nuclear localization of TBPH when knocking out *NFAT* and *CanB*. Interestingly, even though knockout of *Pkc53E* did not result in re-localization of TBPH in the previously published literature, we do still see a rescue of the eclosion defect in the *OK371>TBPH[N493D]* model. However, the density of the vials was low which led to a wide range of eclosion ratios in each of the crosses. It has previously been observed that RNAi silencing of *Cam* failed to relocalize cytoplasmic TBPH to the nucleus in a TDP-43 overexpression model (Park et al., 2020). In turn, we did not see a significant rescue of eclosion by Cam-RNAi in our model. While not significant, two

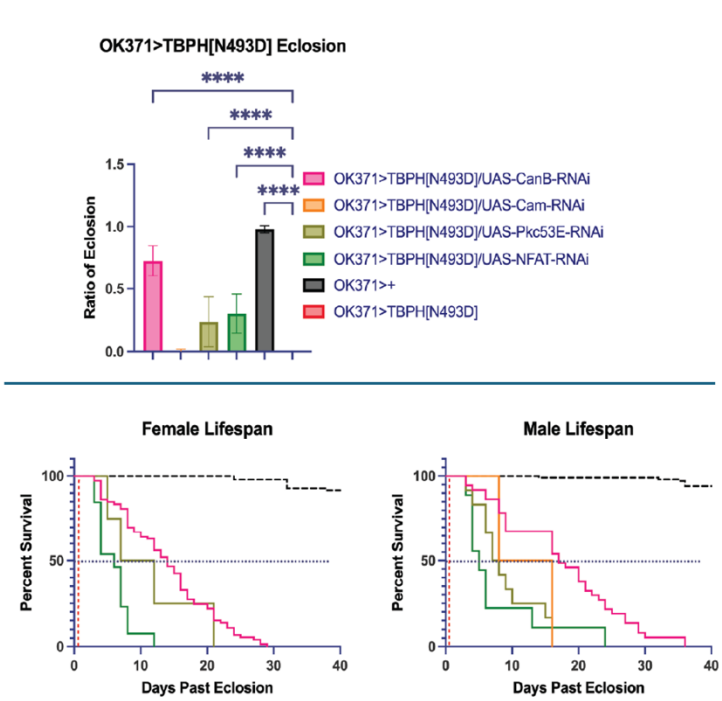

Genotype	♀ Median Survival (days)	♂ Median Survival (days)
OK371>TBPH[N493D]	-	-
OK371>TBPH[N493D]/UAS-CanB-RNAi	14	17
OK371>TBPH[N493D]/UAS-Cam-RNAi	-	12
OK371>TBPH[N493D]/UAS-Pkc53E-RNAi	9.5	7.5
OK371>TBPH[N493D]/UAS-NFAT-RNAi	6	5
OK371>+	70	64

OK371-Gal4	+	+	+	+	+	+
UAS-TBPH[N493D]	–	+	+	+	+	+
UAS-CanB-RNAi	–	–	+	–	–	–
UAS-Cam-RNAi	–	–	–	+	–	–
UAS-Pkc53E-RNAi	–	–	–	–	+	–
UAS-NFAT-RNAi	–	–	–	–	–	+

Figure 3.6: Eclosion and Lifespan Assays of *OK371>TBPH[N493D]* utilizing Ca^{2+}-pathway RNAi's
Lifespans are represented by Kaplan-Meier curves. *OK371>+* (♀n = 97, ♂n=104). *OK371>TBPH[N493D]/CanB-RNAi* (♀n=73, ♂n=37). *OK371>TBPH[N493D]/Cam-RNAi* (♀n=0, ♂n=2). *OK371>TBPH[N493D]/Pkc53E-RNAi* (♀n=4, ♂n=12). *OK371>TBPH[N493D]/NFAT-RNAi* (♀n=13, ♂n=9) All flies raised at 25ºC. Mantel-Cox tests were performed on complete lifespan curves. Eclosion statistical testing: one-way ANOVA, ***p<0.001, ****p<0.0001. Lifespan statistical testing: all comparisons between models for lifespan Mantel-Cox test (p<0.0001).

OK371>TBPH[N493D]/Cam-RNAi males eclosed exhibiting a median lifespan of 2 days.

Further studies may be warranted with other assays to determine the potential involvement of Cam in alleviating ALS-associated phenotypes.

3.8 References

Aktas, T., Avsar Ilik, I., Maticzka, D., Bhardwaj, V., Pessoa Rodrigues, C., Mittler, G., Manke, T., Backofen, R., & Akhtar, A. (2017). DHX9 suppresses RNA processing defects originating from the Alu invasion of the human genome. *Nature*, *544*(7648), 115-119. https://doi.org/10.1038/nature21715

Arnold, E. S., Ling, S. C., Huelga, S. C., Lagier-Tourenne, C., Polymenidou, M., Ditsworth, D., Kordasiewicz, H. B., McAlonis-Downes, M., Platoshyn, O., Parone, P. A., Da Cruz, S., Clutario, K. M., Swing, D., Tessarollo, L., Marsala, M., Shaw, C. E., Yeo, G. W., & Cleveland, D. W. (2013). ALS-Linked TDP-43 mutations produce aberrant RNA splicing and adult-onset motor neuron disease without aggregation or loss of nuclear TDP-43. *PNAS*, E736-E745. https://doi.org/10.1073/pnas.1222809110

Bello, A. I., Goswami, R., Brown, S. L., Costanzo, K., Shores, T., Allan, S., Odah, R., & Mohan, R. D. (2022). Deubiquitinases in Neurodegeneration. *Cells*, *11*(3). https://doi.org/10.3390/cells11030556

Bhogal, J. K., Kanaskie, J. M., & DiAngelo, J. R. (2020). The role of the heterogeneous nuclear ribonucleoprotein (hnRNP) Hrb27C in regulating lipid storage in the Drosophila fat body. *Biochem Biophys Res Commun*, *524*(1), 178-183. https://doi.org/10.1016/j.bbrc.2020.01.064

Bruckert, H., Marchetti, G., Ramialison, M., & Besse, F. (2015). Drosophila Hrp48 Is Required for Mushroom Body Axon Growth, Branching and Guidance. *PLoS One*, *10*(8), e0136610. https://doi.org/10.1371/journal.pone.0136610

Cugusi, S., Kallappagoudar, S., Ling, H., & Lucchesi, J. C. (2015). The Drosophila Helicase Maleless (MLE) is Implicated in Functions Distinct From its Role in Dosage Compensation. *Mol Cell Proteomics*, *14*(6), 1478-1488. https://doi.org/10.1074/mcp.M114.040667

Das, R., Schwintzer, L., Vinopal, S., Aguado Roca, E., Sylvester, M., Oprisoreanu, A. M., Schoch, S., Bradke, F., & Broemer, M. (2019). New roles for the de-ubiquitylating enzyme OTUD4 in an RNA-protein network and RNA granules. *J Cell Sci*, *132*(12). https://doi.org/10.1242/jcs.229252

Fan, A. C., & Leung, A. K. (2016). RNA Granules and Diseases: A Case Study of Stress Granules in ALS and FTLD. *Adv Exp Med Biol*, *907*, 263-296. https://doi.org/10.1007/978-3-319-29073-7_11

Finger, D. S., Williams, A. E., Holt, V. V., & Ables, E. T. (2023). Novel roles for RNA binding proteins squid, hephaesteus, and Hrb27C in Drosophila oogenesis. *Dev Dyn*, *252*(3), 415-428. https://doi.org/10.1002/dvdy.550

Gao, X., Xin, L., Yao, Z., Silvennoinen, O., & Yang, J. (2023). Friend or Foe? The fascinating Tudor-SN protein. *Visualized Cancer Medicine*, *4*. https://doi.org/10.1051/vcm/2023001

Gargano, J. W., Martin, I., Bhandari, P., & Grotewiel, M. S. (2005). Rapid iterative negative geotaxis (RING): a new method for assessing age-related locomotor decline in Drosophila. *Exp Gerontol*, *40*(5), 386-395. https://doi.org/10.1016/j.exger.2005.02.005

Goodman, L. D., Prudencio, M., Kramer, N. J., Martinez-Ramirez, L. F., Srinivasan, A. R., Lan, M., Parisi, M. J., Zhu, Y., Chew, J., Cook, C. N., Berson, A., Gitler, A. D., Petrucelli, L., & Bonini, N. M. (2019). Toxic expanded GGGGCC repeat transcription is mediated by the PAF1 complex in C9orf72-associated FTD. *Nat Neurosci*, *22*(6), 863-874. https://doi.org/10.1038/s41593-019-0396-1

Goodrich, J. S., Clouse, K. N., & Schupbach, T. (2004). Hrb27C, Sqd and Otu cooperatively regulate gurken RNA localization and mediate nurse cell chromosome dispersion in Drosophila oogenesis. *Development*, *131*(9), 1949-1958. https://doi.org/10.1242/dev.01078

Graca, F. A., Sheffield, N., Puppa, M., Finkelstein, D., Hunt, L. C., & Demontis, F. (2021). A large-scale transgenic RNAi screen identifies transcription factors that modulate myofiber size in Drosophila. *PLoS Genet*, *17*(11), e1009926. https://doi.org/10.1371/journal.pgen.1009926

Gutierrez-Beltran, E., Denisenko, T. V., Zhivotovsky, B., & Bozhkov, P. V. (2016). Tudor staphylococcal nuclease: biochemistry and functions. *Cell Death Differ*, *23*(11), 1739-1748. https://doi.org/10.1038/cdd.2016.93

Ho, D. M., Shaban, M., Mahmood, F., Ganguly, P., Todeschini, L., Van Vactor, D., & Artavanis-Tsakonas, S. (2024). cAMP/PKA signaling regulates TDP-43 aggregation and mislocalization. *Proc Natl Acad Sci U S A*, *121*(24), e2400732121. https://doi.org/10.1073/pnas.2400732121

Johnson, D. M., Wells, M. B., Fox, R., Lee, J. S., Loganathan, R., Levings, D., Bastien, A., Slattery, M., & Andrew, D. J. (2020). CrebA increases secretory capacity through direct transcriptional regulation of the secretory machinery, a subset of secretory cargo, and other key regulators. *Traffic*, *21*(9), 560-577. https://doi.org/10.1111/tra.12753

Kankel, M. W., Sen, A., Lu, L., Theodorou, M., Dimlich, D. N., McCampbell, A., Henderson, C. E., Shneider, N. A., & Artavanis-Tsakonas, S. (2020). Amyotrophic Lateral Sclerosis Modifiers in Drosophila Reveal the Phospholipase D Pathway as a Potential Therapeutic Target. *Genetics*, *215*(3), 747-766. https://doi.org/10.1534/genetics.119.302985

Liang, S., Zhu, C., Suo, C., Wei, H., Yu, Y., Gu, X., Chen, L., Yuan, M., Shen, S., Li, S., Sun, L., & Gao, P. (2022). Mitochondrion-Localized SND1 Promotes Mitophagy and Liver Cancer Progression Through PGAM5. *Front Oncol*, *12*, 857968. https://doi.org/10.3389/fonc.2022.857968

Marcelo, A., Koppenol, R., de Almeida, L. P., Matos, C. A., & Nóbrega, C. (2021). Stress granules, RNA-binding proteins and polyglutamine diseases: too much aggregation? *Cell Death & Disease*, *12*(6). https://doi.org/10.1038/s41419-021-03873-8

Markmiller, S., Soltanieh, S., Server, K. L., Mak, R., Jin, W., Fang, M. Y., Luo, E. C., Krach, F., Yang, D., Sen, A., Fulzele, A., Wozniak, J. M., Gonzalez, D. J., Kankel, M. W., Gao, F. B., Bennett, E. J., Lecuyer, E., & Yeo, G. W. (2018). Context-Dependent and Disease-Specific Diversity in Protein Interactions within Stress Granules. *Cell*, *172*(3), 590-604 e513. https://doi.org/10.1016/j.cell.2017.12.032

Morra, R., Yokoyama, R., Ling, H., & Lucchesi, J. C. (2011). Role of the ATPase/helicase maleless (MLE) in the assembly, targeting, spreading and function of the male-specific lethal (MSL) complex of *Drosophila*. *Epigentics & Chromatin*, *4*(6). https://doi.org/10.1186/1756-8935-4-6

Navarro-Imaz, H., Ochoa, B., Garcia-Arcos, I., Martinez, M. J., Chico, Y., Fresnedo, O., & Rueda, Y. (2020). Molecular and cellular insights into the role of SND1 in lipid

metabolism. *Biochim Biophys Acta Mol Cell Biol Lipids*, *1865*(5), 158589. https://doi.org/10.1016/j.bbalip.2019.158589

Park, J. H., Chung, C. G., Park, S. S., Lee, D., Kim, K. M., Jeong, Y., Kim, E. S., Cho, J. H., Jeon, Y. M., Shen, C. J., Kim, H. J., Hwang, D., & Lee, S. B. (2020). Cytosolic calcium regulates cytoplasmic accumulation of TDP-43 through Calpain-A and Importin alpha3. *eLife*, *9*. https://doi.org/10.7554/eLife.60132

Reenan, R. A., Hanrahan, C., J., & Ganetzky, B. (2000). The mle^{napts} RNA Helicase Mutation in *Drosophila* Results in a Splicing Catastrophe of the *para* Na^+ Channel Transcript in a Region of RNA Editing. *Neuron*, *25*, 139-149.

Spierer, A. N., Yoon, D., Zhu, C. T., & Rand, D. M. (2021). FreeClimber: automated quantification of climbing performance in Drosophila. *J Exp Biol*, *224*(Pt 2). https://doi.org/10.1242/jeb.229377

Wang, W., Wang, L., Lu, J., Siedlak, S. L., Fujioka, H., Liang, J., Jiang, S., Ma, X., Jiang, Z., da Rocha, E. L., Sheng, M., Choi, H., Lerou, P. H., Li, H., & Wang, X. (2016). The inhibition of TDP-43 mitochondrial localization blocks its neuronal toxicity. *Nat Med*, *22*(8), 869-878. https://doi.org/10.1038/nm.4130

Wolozin, B., & Ivanov, P. (2019). Stress granules and neurodegeneration. *Nat Rev Neurosci*, *20*(11), 649-666. https://doi.org/10.1038/s41583-019-0222-5

Xu, Z., Poldevin, M., Li, X., Li, Y., Shu, L., Nelson, D. L., Li, H., Hales, C., M., Gearing, M., Wingo, T. S., & Jin, P. (2013). Expanded GGGGCC repeat RNA associated with amyotrophic lateral sclerosis and frontotemporal dementia causes neurodegeneration. *PNAS*, *110*(19), 7778-7783. https://doi.org/10.1073/pnas.1219643110

Yang, S., Wijegunawardana, D., Sheth, U., Veire, A. M., Salgado, J. M. S., Agrawal, M., Zhou, J., Pereira, J. D., Gendron, T. F., & Guo, J. U. (2023). Aberrant splicing exonizes C9ORF72 repeat expansion in ALS/FTD. *bioRxiv*. https://doi.org/10.1101/2023.11.13.566896

Chapter 4 – DISCUSSION AND CONCLUSION

4.1 Discussion of *C9ORF72* Experiments

This thesis characterizes models of *C9ORF72* and TDP-43 ALS in *Drosophila melanogaster* utilizing multiple Gal4 drivers concentrating on specific populations of cells. In characterizing the *C9ORF72* model, two models of G4C2 repeats exhibited very different results in levels of lethality as well as sex specific effects. Our *nSyb>G4C2(49X)* repeat model, while it is capable of adult viability, exhibits sex-specific effects with males being unable to eclose from the pupal case. As we are sorting for progeny using a *CyO* balancer, we are unable to determine whether the male progeny are able to make it through the life cycle to pharate stage and then proceeding to die in the pupal case *or* if they are experiencing lethality earlier in the developmental process. While we would expect a *C9orf72*-ALS model with 49 HRE repeats expressed in all neurons to be more lethal than a model driving 30 HRE repeats in motor neurons only, that does not appear to be the case in our observations. As the 49X model does not contain an AUG start codon in the construct, we would expect increased toxicity. But again, this is not what we observe specifically in females.

One possible explanation for the variances we observe could be due to where the constructs are inserted. While both models contain insertions on the second chromosome, the insertions were random. If the insertion of the 49X repeat model is in a region of the genome with greater density of chromatin, that could also lead to a lack of *UAS* accessibility and expression of the HRE. A third possible mechanism to the higher lethality observed in the 30X model could be the Gal4 used for each of the experiments. While the 49X repeats are pan-neuronal, the *nSyb-Gal4* is expressed later in the developmental cycle relative to the *OK6-Gal4* used in the 30X model. To elucidate the cell-specific effects further, we are currently in the

process of investigating the 49X model with the glutamatergic *OK6-Gal4* and the 30X model with the pan-neuronal *nSyb-Gal4.* This will ensure that we have fully investigated cell targeting effects as well as potential insertion and repeat expansion effects when comparing each of our RNAi's of interest.

In our climbing data in the *nSyb>G4C2(49X)* model, we observe a climbing defect in female flies that progressively worsens throughout their lifespans. It is important to note that there is also progressive motor decline in our WT flies. Although, its decline is much less severe than the disease model (Figure 3.2-A). If we were to repeat these climbing experiments again, we would also better characterize the climbing behaviors observed in the disease model as well as the associated rescues. The behaviors of the experimental flies vary across the lifespan and change dependent on whether or not the G4C2 HRE is present in the line. Some behaviors observed include "popcorning" with rapid and seemingly uncontrolled movements. We also observe a "fishbowl" effect in some lines, with *Drosophila* not taking the most direct route up the side of the vial. Properly documenting the behaviors exhibited in these models would prove to be useful to gain greater understanding of potential reflex and perception impacts that may be present in the experimental progeny.

The rescue observed in climbing velocity is best seen towards the later stages of the disease model lifespan. To better quantify rescue of the disease model, we measured significance in climbing velocity differences from days 1-10 and then from days 10.5 through the end of lifespan. Significant differences in climbing velocity were best observed in the 10.5 through end of lifespan timeframe. Ultimately, a slow-down in motor disease progression is best observed closer to when 50% of the progeny have died. This could be due to a delay in "rescue" whereas silencing of these genes is most effective after a few days of its RNAi being active. It is also

possible that due to the parameters for this experiment, that enhanced presence to stress had different effects on the disease model relative to the disease model with the RNAi's. Considering the amount of climbing conducted in these experiments, it would be insightful to observe whether these same trends continue if we climb the flies less often. An example for future parameters could be determine if we observe the same trends if the flies are only climbed once a day or every other day. Future experiments should better evaluate timeframe of the disease model and single out points of disease development where intervention could be best utilized.

It is also important to identify a proper negative control for our *C9orf72* and TDP-43 experiments. Throughout these assays we utilize a *UAS-LacZ* which does not encode for any gene in the *Drosophila* genome. In each assay tested, we have determined that the addition of a UAS sequence does not rescue any of the disease models used here in regards to lifespan extension nor localization of TBPH. We do observe a rescue earlier in development for *nSyb>G4C2(49);LacZ* in our climbing assay, however we ultimately do not see an extension in lifespan or a slowed rate of motor degeneration. As we are incorporating RNAi's in each of these experiments, it is necessary to identify a control RNAi to validate that the use of an RNAi itself is not influencing any of the experimental results we observe in this thesis. This is especially important as one of our genes of interest utilized in this thesis is *Tudor-SN,* which is a component of the RNA-induced silencing complex (RISC) (Gutierrez-Beltran et al., 2016). In the future, we will utilize RNAi's that have previously been used in larger scale RNAi screens to control for the addition of a RNAi into the model (Graca et al., 2021). Potential control lines identified should also be built from same genetic background as the RNAi's used in this thesis such as utilizing the same chromosome.

We observe an extension in our *nSyb>G4C2(49X)* model when knocking down *Tudor-SN, mle,* and *Hrb27C*. *Hrb27C* and *mle* knockdown also leads to an improvement in climbing velocity in our *G4C2* model. However, while investigating our *OK6>G4C2 (30X)* model, each of these SG-RNAi's rescue the model in addition to *UAS-otu-RNAi.* The cell-specific rescue could be indicative of a specific role that *otu* has pan-neuronally whereas the silencing of *otu* in motor neurons specifically does not appear to be detrimental to the organism. It is also interesting to note that while we do not observe any significant differences in the female median lifespan in the *nSyb>otu-RNAi* line, we do see that males in particular are sensitive to the RNAi silencing of *otu* pan-neuronally (Figure A.7). We also observe this male-specific-defect with our motor neuron drivers *OK371-Gal4* and *OK6-Gal4* (Figure A.8 and A.9). The gene *ovarian tumor* does not have a previously known neuronal-specific role. A majority of the literature focuses on its role in female germline determination and embryonic patterning. Although deubiquitinases, like *otu,* have previously been described as ideal targets for therapeutic intervention in neurodegenerative diseases (Bello et al., 2022).

It is also important to note in our *G4C2(49X)* experiments that knockdown of *mle* resulted in significant lifespan extension and climbing velocity rescue. Interestingly, without the disease model background, there is a much starker difference in lifespan with analysis of *nSyb>mle-RNAi* (Figure A-7). Knockdown of *mle* in males and in females without the disease model appears to have a significant detrimental effect relative to the other control RNAi's tested. It is important to repeat these crosses to validate these results and that work is ongoing. This is especially needed as the median lifespans are so similar between *nSyb>G4C2(49X);mle-RNAi* and *nSyb>mle-RNAi.* However, we will note that each of the crosses included in these experiments were set up in triplicate. qPCR validation of the *UAS-mle-RNAi* line is ongoing as

well. However, between the *nSyb>G4C2(49X)* and the *OK6>G4C2(30X)* models we do see a rescue with *mle* knockdown. This identifies a rescue with multiple disease models and cellular population targets. The previously known roles for *mle* include dosage compensation, specifically as it is a member of the Male-Specific-Lethal (MSL) dosage compensation complex. However, it also has shown to associate to ribonucleoproteins involved in RNA processing (including another SG-associated gene studied in this thesis, *Hrb27C*) and in regulating spliceosome function (Cugusi et al., 2015). Aberrant splicing is a hallmark of *C9orf72* ALS and splicing of the *C9orf72* gene is heavily altered in motor neurons in mammalian ALS (Yang et al., 2023). Aberrant splicing is also observed in TDP-43 ALS, providing another avenue to explore similarities of mechanisms between the disease models as well as routes of action when investigating potential genes of interest for rescue, like *mle* (Arnold et al., 2013).

Throughout each of these experiments, we consistently observe an adult-functional rescue upon silencing of *Hrb27C*. The only experiment where we observe a failure of *Hrb27C-RNAi* to rescue the disease model is through assessment of TBPH cytoplasmic localization in the larval VNC (Figure A.12). *Hrb27C* is commonly known as an RNA-binding protein and had already been identified to localize to stress granules prior to the APEX-labeling study conducted in Markmiller et al (Markmiller et al., 2018). *Hrb27C* has an essential role in embryonic patterning, lipid metabolism, and RNA processing. At the protein level, it has exhibited a multitude of physical and biological interactions. Finally, its mammalian ortholog (*DAZAP1, Hrp48*) has demonstrated a functional role in dendritic morphology of mushroom bodies (Bruckert et al., 2015). *Hrb27C* has also already been identified to interact with other genes identified in this thesis, such as *otu*. With its successful usage across cell populations and targets, it is a promising target to investigate further. In addition to including other *UAS-Hrb27C-RNAi*

lines in each of these experiments to validate these findings, we have also sourced other alleles for *Hrb27C* to include to this dataset. We want to confirm that any results observed here is not due to the use of this particular RNAi line.

4.2 Discussion of TDP-43 ALS

In our experiments, we do see a rescue in adult viability of the *OK371>TBPH[N493D]* model when knocking down *otu, Hrb27C,* and *mle* but not with *Tudor-SN* knockdown. This could be due to the stock itself that was used as it has been common to observe a lack of progeny overall when *Tudor-SN* is knocked down. However, it could also be due to the mechanism of toxicity of the model itself. Mislocalization of TDP-43 protein to the cytoplasm is a key hallmark of ALS. It is curious that movement of TBPH protein into the nucleus does not appear to rescue the motor defects observed in the disease model in the case of *Tudor-SN* silencing. There are other molecular underpinnings that are potentially contributing to the phenotypes we observe in the disease model aside from mislocalization of TBPH. I have previously addressed the need to study aberrant splicing in both of our ALS models via RNA sequencing. Another point of interest for the future, would be investigating TDP-43 localization in other components of the cell. For example, TDP-43 has shown to aggregate to the mitochondria of neurons in patients with ALS and FTD (Wang et al., 2016). In mammals, Tudor-SN protein has been shown to localize to mitochondria and critically regulate mitophagy (Liang et al., 2022). Future experiments should investigate other mechanisms and other cellular activities that *Tudor-SN* could be acting upon. This screening of additional cellular mechanisms could also help elucidate rescues that are observed with silencing of other stress granule-associated genes.

As TDP-43 localization in the cytoplasm is a core component of the ALS model, it was especially interesting that we observe rescue of these ALS motor defects with knockdown of *otu, mle,* and *Hrb27C.* We have confirmed with qPCR that *TBPH* gene expression is higher relative to WT in the *OK371>TBPH[N493D]* disease model. We have also observed that knockdown of *otu* within the *OK371>TBPH[N493D]* model does reduce *TBPH* expression, but not the extent of a *TBPH-RNAi* utilized in the disease model background (Figure A.11-A). While this assay is investigating transcriptional effects, we have yet to quantify protein levels in the disease model. There is also a need to further investigate TBPH at the protein level with the utilization of RNAi's. We also observe some differences in TBPH signal intensity between genotypes through experimental microscopy (Figure 3.5). It is especially important to further investigate TBPH quantitative levels between genotypes and whether TBPH protein is being upregulated or downregulated across genotypes.

Knockdown of *Tudor-SN* results in the re-localization of TBPH back to the nucleus. However, as previously mentioned, we do not observe rescue of the *OK371>TBPH[N493D]* model in an assessment of the disease model eclosion defect with *Tudor-SN* silencing. We are currently investigating other *Tudor-SN* alleles including a deficiency and two null alleles in regards to whether we observe similar results with these other alleles of *Tudor-SN* (Johnson et al., 2020). This will include an assessment of the TBPH localization in the VNC as well as an eclosion assessment. It is essential to verify that any results observed with *Tudor-SN* is not solely due to the presence of the RNAi, but rather is in relation to the transcriptional expression of the gene itself. As *Tudor-SN* has been previously identified as a member of the RNA-induced silencing complex (RISC), it is especially important to verify that its silencing is not also having an impact on RNAi function itself. It should be noted, that we have verified *Tudor-SN* silencing

with a *Tubulin-Gal4* driver in 3rd-instar wandering larvae (Figure A.11-C). We will also verify the expression levels of these other *Tudor-SN* alleles.

It is not clear as to why *Tudor-SN* silencing improves the mislocalization of TBPH in our *OK371>TBPH[N493D]* model. It is possible that TBPH is physically binding to Tudor-SN protein, which is contributing to the results observed and effectively removing these cytoplasmic aggregates. We do observe TBPH in the cytoplasm as well as a much stronger signal of anti-TBPH in the *OK371>TBPH[N493D]* disease model relative to the WT. As mentioned earlier in this section, we would like to also quantify TBPH levels at this stage in development. It is also possible that *Tudor-SN* has a more integral role in stress granule assembly. However, no previous literature has identified *Tudor-SN* as a SG-core-recruiter in any species. We could also be influencing TBPH localization indirectly by either upregulating or downregulating another component that is more heavily involved in TBPH localization. There are physical and biological interactors with *Tudor-SN* that have previously been documented and investigating knockdowns of other biological interactors of this gene could prove beneficial to investigate pathways of action. Future experiments should include transcriptomics on our *Tudor-SN-RNAi* or other *Tudor-SN* alleles to identify any differential expression patterns relative to WT. We have attempted to investigate one possible reason for TBPH re-localization by investigating particular calcium pathways that have already demonstrated their ability or inability to mobilize TBPH (Figure 3.7). We are also in the process of confirming the TBPH localization observed in Park et al. (Park et al., 2020). To investigate cytosolic calcium levels upon knockdown of *Tudor-SN*, we will pursue quantification of cytosolic calcium levels in the *OK371>TBPH[N493D]* model. There is no prior literature identifying a calcium-regulatory function for the gene *Tudor-SN*. Finally, we would also like to investigate the *OK371>TBPH[WT]* line and quantify any

difference that might be present between an overexpression of the WT TBPH protein vs. an overexpression of the mutated [N493D] protein.

As the four genes described here encode proteins that are components of stress granules, it is also important to further investigate stress granule dynamics in each of the ALS models described in this thesis. While *otu, Hrb27C, Tudor-SN*, and *mle* have well established roles outside of their potential roles in stress granules, stress granule dynamics in an *in vivo Drosophila* model have not been well investigated. Two core components of stress granules are the proteins RIN (dG3BP1) and ATXN2. Future experiments should investigate RIN and ATXN2 localization and quantity across the *C9orf72* and TDP-43 models. We would expect for each of the four stress granule components to associate with RIN and/or ATXN2 due to their association to stress granules. We have yet to determine the status of stress granules within an *in vivo* model and whether these dynamics vary between cellular populations and/or time in development. For example, in our *OK371>TBPH[N493D]* model, we are assessing the disease model at the larval stage in development. It is important to examine if stress granule presence and quantity is varied from larval to pharate to adult stage and if we observe differences in the brain versus the neuromuscular junction and/or the legs. Measuring RIN and ATXN2 levels and localization could help elucidate whether silencing of any of the four genes described in this thesis are directly affecting stress granule dynamics in an *in vivo* model. We can also investigate physical binding between either of these SG markers and our proteins of interest.

4.3 Conclusion

We have characterized effects of multiple *Drosophila* models of ALS upon knockdown of genes that encode stress granule-associating proteins. These assessments include adult

viability, lifespan, and climbing velocity as a measure of motor function. We have determined that knockdown of *Hrb27C*, *Tudor-SN,* and *mle* rescue a pan-neuronal and motor neuron model of *C9orf72*-ALS however *Tudor-SN* silencing does not greatly improve the observed defect in climbing. To determine whether this lifespan extension can be observed in another model of ALS, we overexpressed the mutant TBPH protein through our *OK371>TBPH[N493D]* model. Here, we observe that knockdown of *otu, Hrb27C,* and *mle* rescue the eclosion defect in the disease model and significantly extend the lifespan of the model. We also quantified the effect of stress granule-associated gene knockdown on the localization of TBPH protein. Interestingly, we observe that knockdown of *Tudor-SN* results in re-localization of TBPH back into the nucleus in motor neurons. Finally, we attempt to identify the mechanism that this TBPH re-localization is acting on by utilizing RNAi's of modifiers to Ca^{2+} pathways. We observe that while two pathways that have previously shown to move TBPH to the nucleus are able to rescue an *OK371>TBPH[N493D]* eclosion defect, there are other RNAi's that can rescue this defect and are unable to move TBPH out of the cytoplasm. The findings in this thesis provide new insights into the roles of stress granules and ALS and identifies potential therapeutic targets for this neurodegenerative disease.

4.4 References

Arnold, E. S., Ling, S. C., Huelga, S. C., Lagier-Tourenne, C., Polymenidou, M., Ditsworth, D., Kordasiewicz, H. B., McAlonis-Downes, M., Platoshyn, O., Parone, P. A., Da Cruz, S., Clutario, K. M., Swing, D., Tessarollo, L., Marsala, M., Shaw, C. E., Yeo, G. W., & Cleveland, D. W. (2013). ALS-Linked TDP-43 mutations produce aberrant RNA splicing and adult-onset motor neuron disease without aggregation or loss of nuclear TDP-43. *PNAS*, E736-E745. https://doi.org/10.1073/pnas.1222809110

Bello, A. I., Goswami, R., Brown, S. L., Costanzo, K., Shores, T., Allan, S., Odah, R., & Mohan, R. D. (2022). Deubiquitinases in Neurodegeneration. *Cells*, *11*(3). https://doi.org/10.3390/cells11030556

Bruckert, H., Marchetti, G., Ramialison, M., & Besse, F. (2015). Drosophila Hrp48 Is Required for Mushroom Body Axon Growth, Branching and Guidance. *PLoS One*, *10*(8), e0136610. https://doi.org/10.1371/journal.pone.0136610

Cugusi, S., Kallappagoudar, S., Ling, H., & Lucchesi, J. C. (2015). The Drosophila Helicase Maleless (MLE) is Implicated in Functions Distinct From its Role in Dosage Compensation. *Mol Cell Proteomics*, *14*(6), 1478-1488. https://doi.org/10.1074/mcp.M114.040667

Graca, F. A., Sheffield, N., Puppa, M., Finkelstein, D., Hunt, L. C., & Demontis, F. (2021). A large-scale transgenic RNAi screen identifies transcription factors that modulate myofiber size in Drosophila. *PLoS Genet*, *17*(11), e1009926. https://doi.org/10.1371/journal.pgen.1009926

Gutierrez-Beltran, E., Denisenko, T. V., Zhivotovsky, B., & Bozhkov, P. V. (2016). Tudor staphylococcal nuclease: biochemistry and functions. *Cell Death Differ*, *23*(11), 1739-1748. https://doi.org/10.1038/cdd.2016.93

Johnson, D. M., Wells, M. B., Fox, R., Lee, J. S., Loganathan, R., Levings, D., Bastien, A., Slattery, M., & Andrew, D. J. (2020). CrebA increases secretory capacity through direct transcriptional regulation of the secretory machinery, a subset of secretory cargo, and other key regulators. *Traffic*, *21*(9), 560-577. https://doi.org/10.1111/tra.12753

Liang, S., Zhu, C., Suo, C., Wei, H., Yu, Y., Gu, X., Chen, L., Yuan, M., Shen, S., Li, S., Sun, L., & Gao, P. (2022). Mitochondrion-Localized SND1 Promotes Mitophagy and Liver Cancer Progression Through PGAM5. *Front Oncol*, *12*, 857968. https://doi.org/10.3389/fonc.2022.857968

Markmiller, S., Soltanieh, S., Server, K. L., Mak, R., Jin, W., Fang, M. Y., Luo, E. C., Krach, F., Yang, D., Sen, A., Fulzele, A., Wozniak, J. M., Gonzalez, D. J., Kankel, M. W., Gao, F. B., Bennett, E. J., Lecuyer, E., & Yeo, G. W. (2018). Context-Dependent and Disease-Specific Diversity in Protein Interactions within Stress Granules. *Cell*, *172*(3), 590-604 e513. https://doi.org/10.1016/j.cell.2017.12.032

Park, J. H., Chung, C. G., Park, S. S., Lee, D., Kim, K. M., Jeong, Y., Kim, E. S., Cho, J. H., Jeon, Y. M., Shen, C. J., Kim, H. J., Hwang, D., & Lee, S. B. (2020). Cytosolic calcium regulates cytoplasmic accumulation of TDP-43 through Calpain-A and Importin alpha3. *eLife*, *9*. https://doi.org/10.7554/eLife.60132

Wang, W., Wang, L., Lu, J., Siedlak, S. L., Fujioka, H., Liang, J., Jiang, S., Ma, X., Jiang, Z., da Rocha, E. L., Sheng, M., Choi, H., Lerou, P. H., Li, H., & Wang, X. (2016). The inhibition of TDP-43 mitochondrial localization blocks its neuronal toxicity. *Nat Med*, *22*(8), 869-878. https://doi.org/10.1038/nm.4130

Xu, Z., Poldevin, M., Li, X., Li, Y., Shu, L., Nelson, D. L., Li, H., Hales, C., M., Gearing, M., Wingo, T. S., & Jin, P. (2013). Expanded GGGGCC repeat RNA associated with amyotrophic lateral sclerosis and frontotemporal dementia causes neurodegeneration. *PNAS*, *110*(19), 7778-7783. https://doi.org/10.1073/pnas.1219643110

Yang, S., Wijegunawardana, D., Sheth, U., Veire, A. M., Salgado, J. M. S., Agrawal, M., Zhou, J., Pereira, J. D., Gendron, T. F., & Guo, J. U. (2023). Aberrant splicing exonizes C9ORF72 repeat expansion in ALS/FTD. *bioRxiv*. https://doi.org/10.1101/2023.11.13.566896

Chapter 5 - APPENDIX FIGURES

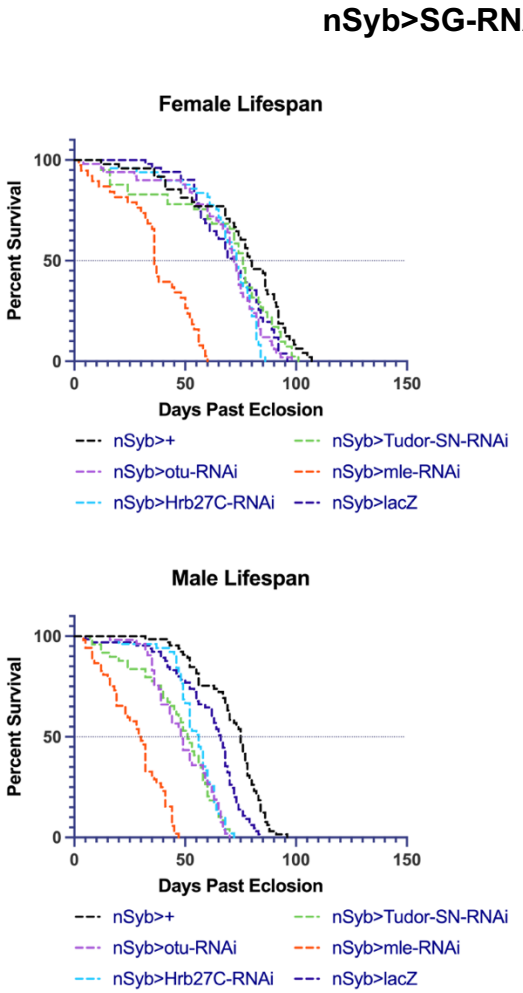

Genotype	♀ *Median Survival (days)*	♂ *Median Survival (days)*
nSyb>+	79.5	75
nSyb>otu-RNAi	72	48
nSyb>Hrb27C-RNAi	73	56
nSyb>Tudor-SN-RNAi	76	51
nSyb>mle-RNAi	36	29.5
nSyb>lacZ	73	66

Figure A.7: Lifespan Assay of Control for nSyb>G4C2(49X) Experiments. Lifespans are represented by Kaplan-Meier curves. *nSyb-Gal4* (♀n = 48, ♂n=65). *nSyb-Gal4>UAS-otu-RNAi* (♀n=50, ♂n=53*). nSyb-Gal4>UAS-Hrb27C-RNAi* (♀n=49, ♂n=51). *nSyb-Gal4>UAS-Tudor-SN-RNAi* (♀n=41, ♂n=49). *nSyb-Gal4>UAS-mle-RNAi* (♀n=38, ♂n=52). *nSyb-Gal4>UAS-lacZ* (♀n=51, ♂n=65). Mantel-Cox tests were performed on complete lifespan curves. All comparisons between models ($p<0.0001$).

nSyb>SG-RNAi Climbing Assay

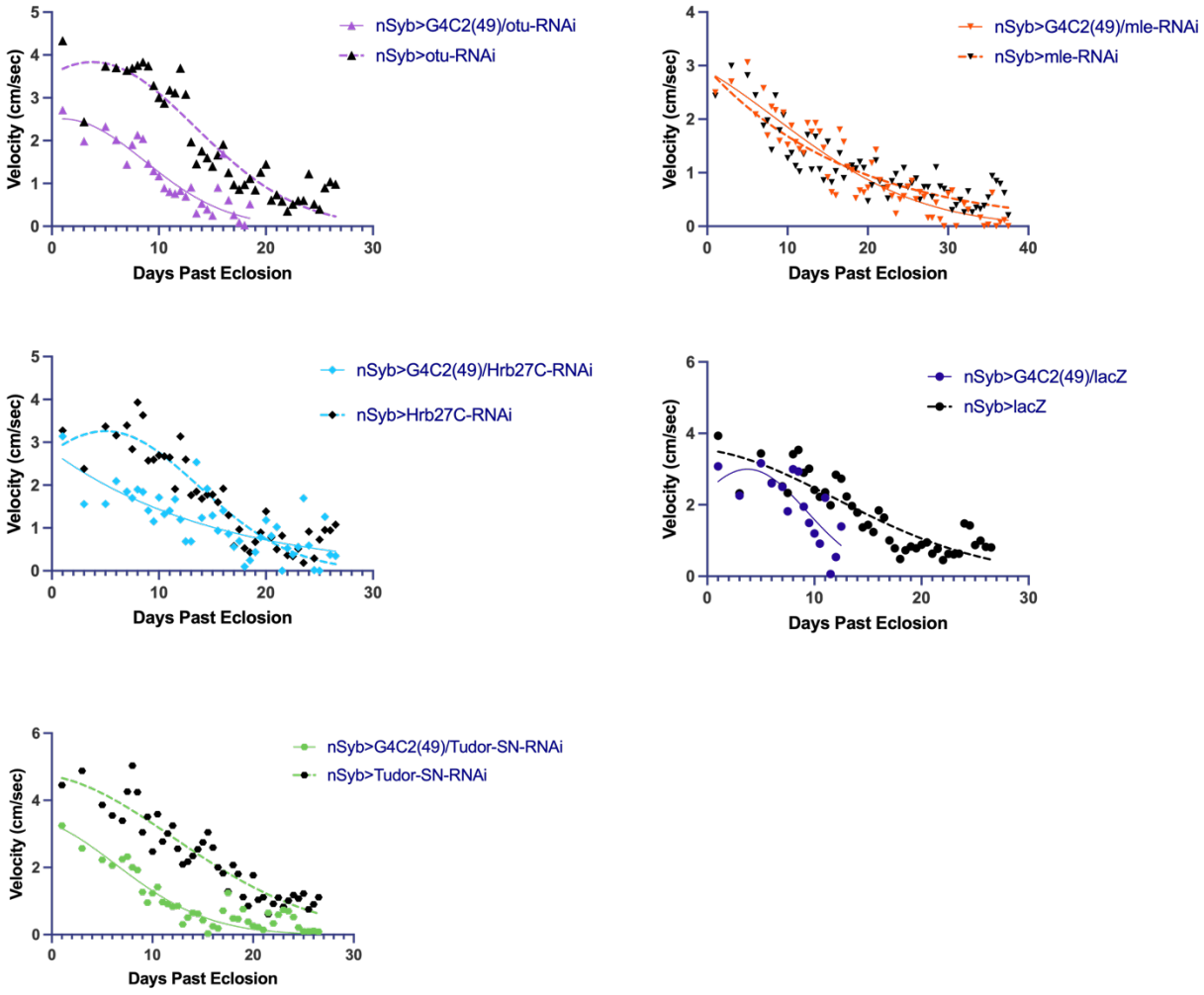

Figure A.8: Climbing Assay of nSyb>G4C2(49X);SG-RNAi vs nSyb>SG-RNAi. Geometric means are presented of technical replicates of vials consisting of ~5 females per vial. Flies were climbed once a day on Days 1, 3, 5, and 6 after eclosion. Flies were climbed twice a day beginning on Day 7. All flies raised at 25ºC. Starting n=50. Solid lines represent Gaussian non-linear regressions with G4C2(49X) disease model background. Dotted lines represent Gaussian non-linear regressions without disease model background. No statistical analyses were performed. Software for data collection and analysis can be found in Spierer et al., 2021.

Timepoint (Day)	P value	Mean of *nSyb>+*	Mean of *nSyb>G4C2(49)*
1	0.502226	4.329	4.015
3	0.508349	2.439	2.062
5	0.004528	3.735	2.082
6	0.000783	3.704	2.012
7	0.000816	3.64	1.635
7.5	0.000043	3.69	1.478
8	0.000047	3.756	1.784
8.5	0.000108	3.83	1.597
9	0.000042	3.743	1.082
9.5	0.000008	3.287	1.382
10	0.000088	3.007	0.7262
10.5	0.000005	2.871	0.805
11	<0.000001	3.18	0.3437
11.5	<0.000001	3.113	0.522
12	0.000001	3.688	0.5926
12.5	0.000031	3.082	0.627
13	0.069069	1.968	0.8027
13.5	0.001859	1.458	0.2237
14	0.002904	1.561	0.1687
14.5		1.598	0

Table A.5: Unpaired t-test comparison of *nSyb>+* vs *nSyb>G4C2(49)* with Welch correction.

Timepoint (Day)	P value	Mean of *nSyb>G4C2(49);otu-RNAi*	Mean of *nSyb>G4C2(49)*
1	0.008236	2.714	4.015
3	0.891662	1.986	2.062
5	0.425487	2.325	2.082
6	0.982615	2.020	2.012
7	0.511060	1.442	1.635
7.5	0.094106	1.901	1.478
8	0.217237	2.133	1.784
8.5	0.177170	2.043	1.597
9	0.183049	1.465	1.082
9.5	0.799858	1.296	1.382
10	0.038834	1.173	0.7262
10.5	0.665951	0.8946	0.805
11	0.092822	0.8063	0.3437
11.5	0.234823	0.7656	0.522
12	0.576161	0.8327	0.5926
12.5	0.877713	0.6992	0.627
13	0.891066	0.912	0.8027

13.5	0.773334	0.3058	0.2237
14	0.383183	0.5318	0.1687
14.5		0.3979	0

Table A.6: Unpaired t-test comparison of *nSyb>G4C2(49);otu-RNAi* vs *nSyb>G4C2(49)* with Welch correction.

Timepoint (Day)	P value	Mean of *nSyb>G4C2(49);Hrb27C-RNAi*	Mean of *nSyb>G4C2(49)*
1	0.130374	3.139	4.015
3	0.35975	1.555	2.062
5	0.142432	1.559	2.082
6	0.82126	2.095	2.012
7	0.59294	1.849	1.635
7.5	0.485908	1.696	1.478
8	0.697917	1.897	1.784
8.5	0.345706	1.839	1.597
9	0.397396	1.407	1.082
9.5	0.564559	1.153	1.382
10	0.202212	1.709	0.7262
10.5	0.415207	1.323	0.805
11	0.227135	1.401	0.3437
11.5	0.316484	1.668	0.522
12	0.299556	1.199	0.5926
12.5	0.910773	0.6861	0.627
13	0.894252	0.6841	0.8027
13.5		2.536	0.2237
14	0.044058	1.235	0.1687
14.5			0

Table A.7: Unpaired t-test comparison of *nSyb>G4C2(49);Hrb27C-RNAi* vs *nSyb>G4C2(49)* with Welch correction.

Timepoint (Day)	P value	Mean of *nSyb>G4C2(49);Tudor-SN-RNAi*	Mean of *nSyb>G4C2(49)*
1	0.133422	3.249	4.015
3	0.353147	2.567	2.062
5	0.709635	2.229	2.082
6	0.916995	2.062	2.012
7	0.176811	2.245	1.635
7.5	0.049368	2.321	1.478
8	0.643765	2.004	1.784
8.5	0.448536	1.921	1.597
9	0.630067	1.267	1.082

9.5	0.158058	0.9503	1.382
10	0.062721	1.231	0.7262
10.5	0.065801	1.416	0.805
11	0.083857	0.966	0.3437
11.5	0.171094	0.9137	0.522
12	0.555975	0.831	0.5926
12.5	0.628717	0.8549	0.627
13	0.361991	0.3089	0.8027
13.5	0.416837	0.5087	0.2237
14	0.237679	0.648	0.1687
14.5		0.6201	0

Table A.8: Unpaired t-test comparison of *nSyb>G4C2(49);Tudor-SN-RNAi* vs *nSyb>G4C2(49)* with Welch correction.

Timepoint (Day)	P value	Mean of *nSyb>G4C2(49);mle-RNAi*	Mean of *nSyb>G4C2(49)*
1	0.009236	2.498	4.015
3	0.236981	2.703	2.062
5	0.043458	3.061	2.082
6	0.874927	2.088	2.012
7	0.175618	2.578	1.635
7.5	0.397805	1.696	1.478
8	0.327457	2.233	1.784
8.5	0.163636	2.167	1.597
9	0.100409	1.595	1.082
9.5	0.146053	2.123	1.382
10	0.002123	1.523	0.7262
10.5	0.008120	1.88	0.805
11	0.002902	1.573	0.3437
11.5	0.003845	1.441	0.522
12	0.068623	1.369	0.5926
12.5	0.066821	1.93	0.627
13	0.112293	1.763	0.8027
13.5	0.000063	1.927	0.2237
14	0.001784	1.767	0.1687
14.5		1.466	0

Table A.9: Unpaired t-test comparison of *nSyb>G4C2(49);mle-RNAi* vs *nSyb>G4C2(49)* with Welch correction

Timepoint (Day)	P value	Mean of *nSyb>G4C2(49);lacZ*	Mean of *nSyb>G4C2(49)*
1	0.066146	3.077	4.015
3	0.740778	2.257	2.062
5	0.025431	3.162	2.082
6	0.331553	2.601	2.012
7	0.320711	2.503	1.635
7.5	0.194891	1.82	1.478
8	0.025562	2.998	1.784
8.5	0.069332	2.934	1.597
9	0.035006	1.947	1.082
9.5	0.910389	1.491	1.382
10	0.150687	1.198	0.7262
10.5	0.784892	0.9132	0.805
11	0.530893	2.2	0.3437
11.5	0.028789	0.06410	0.522
12	0.938030	0.5381	0.5926
12.5	0.679634	1.393	0.627
13			0.8027
13.5			0.2237
14			0.1687
14.5			0

Table A.10: Unpaired t-test comparison of *nSyb>G4C2(49);lacZ* vs *nSyb>G4C2(49)* with Welch correction

OK6>SG-RNAi Lifespan

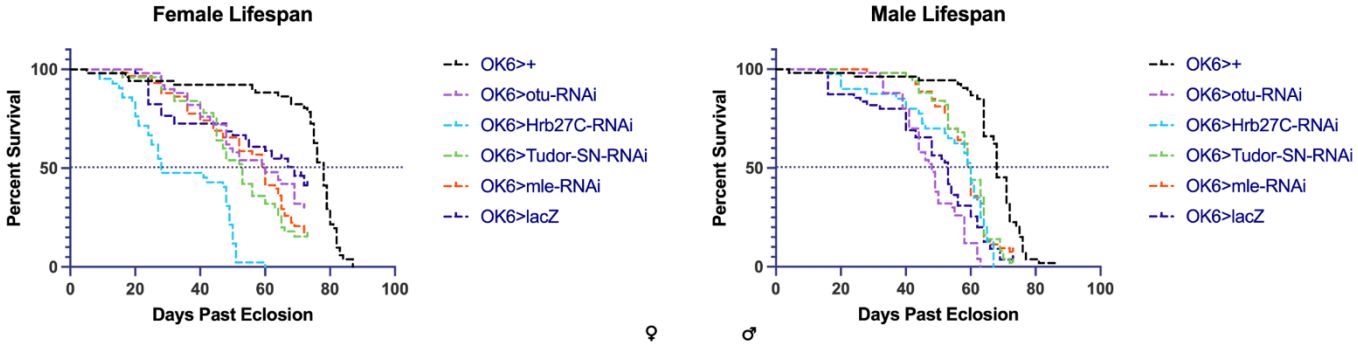

Genotype	♀ Median Survival (days)	♂ Median Survival (days)
OK6>+	78	68
OK6>UAS-otu-RNAi	60	48
OK6>UAS-Hrb27C-RNAi	28	60
OK6>Tudor-SN-RNAi	53	59.5
OK6>UAS-mle-RNAi	59.5	60
OK6>UAS-lacZ	69	53

Figure A.9: Lifespan Assay of Control for OK6>G4C2(30X) Experiments. Lifespans are represented by Kaplan-Meier curves. *OK6-Gal4* (♀ n = 51, ♂n=53). *OK6-Gal4>UAS-otu-RNAi* (♀n=50, ♂n=50*). OK6-Gal4>UAS-Hrb27C-RNAi* (♀n=42, ♂n=40). *OK6-Gal4>UAS-Tudor-SN-RNAi* (♀n=50, ♂n=50). *OK6-Gal4>UAS-mle-RNAi* (♀n=58, ♂n=53). *OK6-Gal4>UAS-lacZ* (♀n=51, ♂n=55). Mantel-Cox tests were performed on complete lifespan curves. All comparisons between models ($p<0.0001$).

OK371>SG-RNAi Lifespan

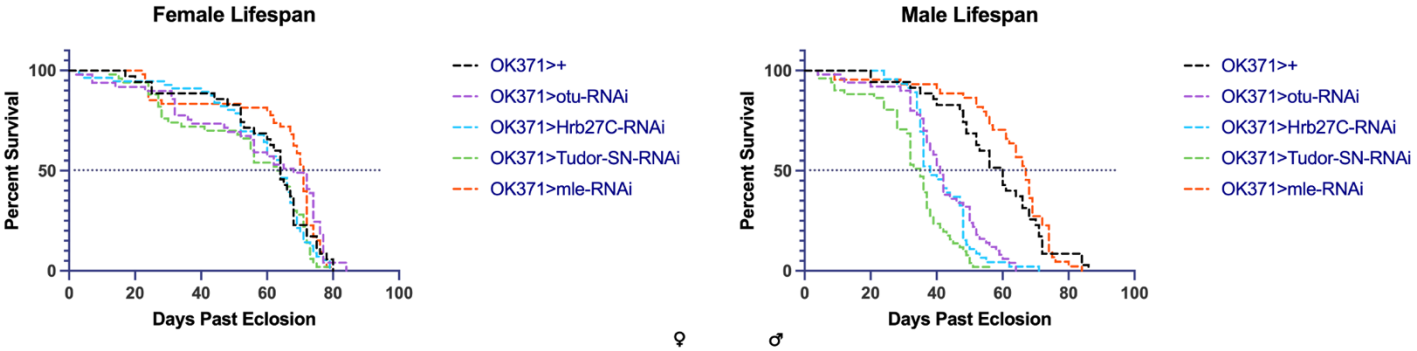

Genotype	♀ *Median Survival (days)*	♂ *Median Survival (days)*
OK371>+	64	60
OK371>UAS-otu-RNAi	68	41
OK371>UAS-Hrb27C-RNAi	64	38
OK371>Tudor-SN-RNAi	63.5	35
OK371>UAS-mle-RNAi	71	67

Figure A.10: Lifespan Assay of Control for OK371>TBPH[N493D] Experiments. Lifespans are represented by Kaplan-Meier curves. *OK371-Gal4* (♀n = 35, ♂n=35). *OK371-Gal4>UAS-otu-RNAi* (♀n=49, ♂n=50*). OK371-Gal4>UAS-Hrb27C-RNAi* (♀n=56, ♂n=46). *OK371-Gal4>UAS-Tudor-SN-RNAi* (♀n=50, ♂n=51). *OK371-Gal4>UAS-mle-RNAi* (♀n=44, ♂n=53). Mantel-Cox tests were performed on complete lifespan curves. All comparisons between models for males ($p<0.0001$) All comparisons between models for females ($p<0.05$).

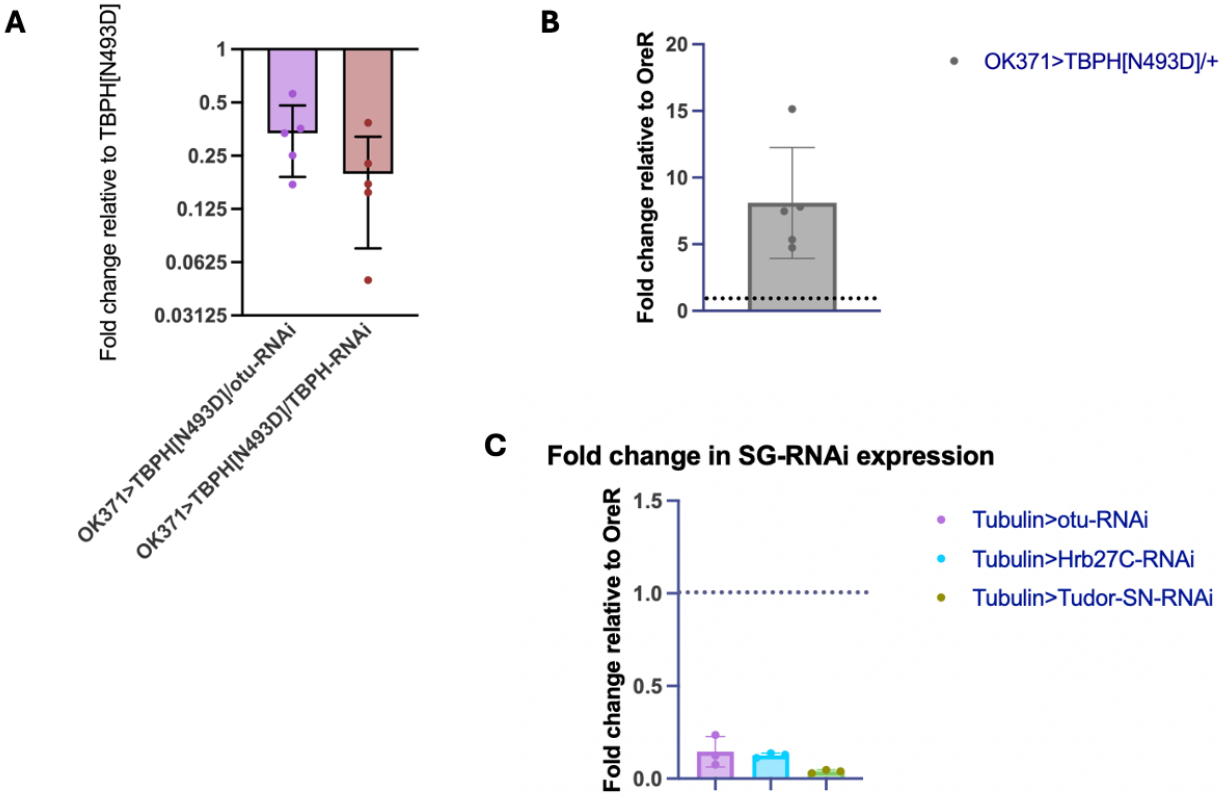

Figure A.11: qPCR Experiments for Gene Expression Validation. Panel A: Quantification of *tbph* expression via qPCR. Fold change is plotted relative to *TBPH* expression in *OK371-Gal4>UAS-TBPH[N493D]/+*. *RP49* used as reference. Columns representative of median. Each data point is representative of three technical replicates per biological replicate. Five biological replicates run. VNC's of third instar wandering larvae were collected. n≥15 per biological replicate. Panel B: Quantification of *TBPH* expression via qPCR. Fold change is plotted relative to *TBPH* expression in OK371>+. *RP49* used as reference. Each data point is representative of three technical replicates. Five biological replicates run. VNC's of third instar wandering larvae were collected. n≥15 per biological replicate. Panel C: Quantification of SG-genes with *RP49* expression used as reference relative to Tubulin>+. Each data point is representative of three technical replicates. Three biological replicates run. Whole third instar wandering larvae were collected. N=6 per biological replicate.

TBPH localization in OK371>TBPH[N493D]/SG-RNAi

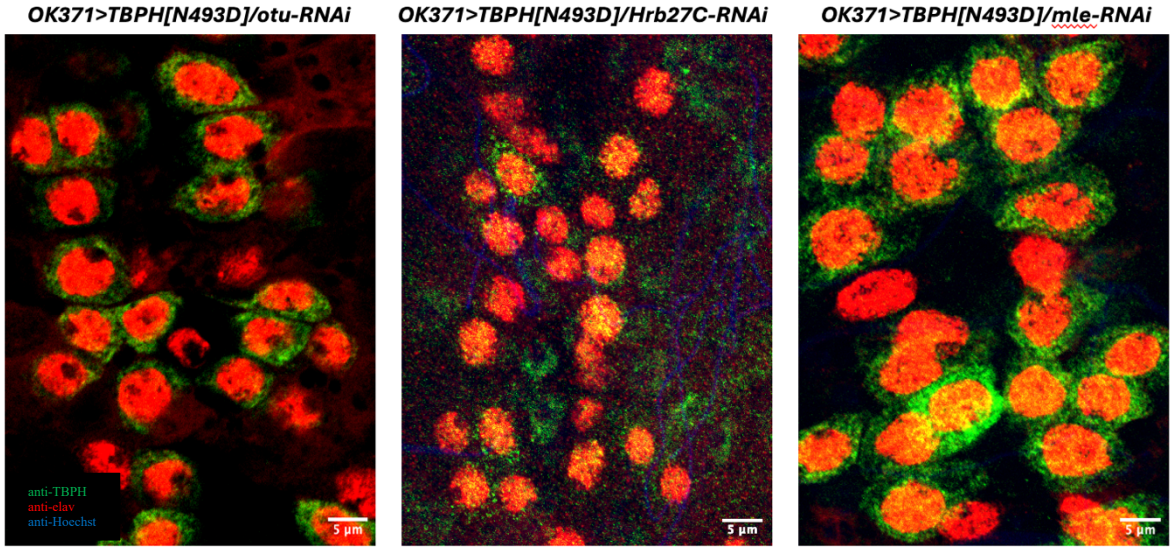

Figure A.12: Cellular TBPH localization in *OK371>TBPH[N493D]* Midline Dorsal Motor Neurons All images are 0.25-micron slices taken at 63X oil. Both channels were adjusted for brightness and contrast.

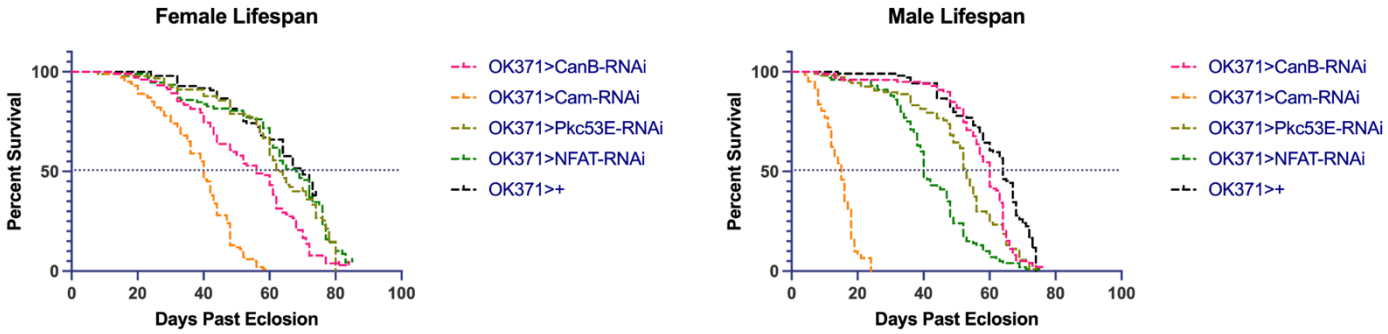

Genotype	♀ *Median Survival (days)*	♂ *Median Survival (days)*
OK371>+	70	64
OK371>UAS-CanB-RNAi	56	60
OK371>UAS-Cam-RNAi	40	15
OK371>UAS-Pkc53E-RNAi	63	53
OK371>UAS-NFAT-RNAi	68.5	40

Figure A.13: Lifespan Assays of *OK371*> Ca^{2+}-pathway RNAi's Lifespans are represented by Kaplan-Meier curves. *OK371*>+ (♀n = 97, ♂n=104). *OK371>CanB-RNAi* (♀n=102, ♂n=99). *OK371>Cam-RNAi* (♀n=100, ♂n=61). *OK371>Pkc53E-RNAi* (♀n=90, ♂n=107). *OK371>NFAT-RNAi* (♀n=92, ♂n=100) All flies raised at 25ºC. Mantel-Cox tests were performed on complete lifespan curves. Lifespan statistical testing: all comparisons between models for lifespan Mantel-Cox test ($p<0.0001$).